PROVER: PRECISION-INDEXED RISK ORDER VIA EUCLIDEAN REACHABILITY IN GAUSSIAN-AFFINE FLOW DECODING

Anonymous authors
Paper under double-blind review

ABSTRACT

When does one source representation supply more useful information than another for velocity prediction? Classical comparison settles this when one representation is a random degradation of the other, but leaves many pairs unordered. We prove an exact order for flows that linearly mix a target with Gaussian noise. At each noise precision, a matrix records the posterior error removed by the representation. Matrix dominance at every precision is equivalent to no larger optimal Euclidean velocity risk on every complete flow. The new step is Euclidean reachability: any positive precision and error metric can be realized together on a normalized noise-to-data path. Complete flows therefore test the full Gaussian-affine quadratic prediction order. This comparison principle also orders frozen predictors with fitting error included and determines when a preferred system remains preferable throughout a prescribed path family.

1 INTRODUCTION

Flow matching learns a velocity by squared-error prediction (Lipman et al., 2023). A representation of source observations—a *report*—provides side information for that prediction. Its value depends on what the noisy state already reveals and which remaining errors the velocity objective emphasizes. Changing the coefficient path changes these questions, even when the target and reports stay fixed. We ask when a preference between reports survives such changes. An exact answer identifies both a common winner and the objectives that can overturn a preference.

Classical theory explains how to compare information. Conditional projection gives the best squared-error predictor for a fixed observation. Blackwell comparison guarantees a common preference across all decision problems when one report can be obtained by random degradation of the other (Blackwell, 1951; 1953; Torgersen, 1991). When neither report can be degraded into the other, it leaves the choice open. Gaussian estimation theory describes prediction error as noise precision changes (Guo et al., 2005; Palomar & Verdú, 2006; Guo et al., 2011). The missing step is geometric: which error comparisons can a *complete flow* realize, when its noisy state and velocity must arise from the same noise-to-data path?

PROVER proves that complete Gaussian-affine flows form a *complete test class* for quadratic information comparison. The new step is *Euclidean reachability*: any positive precision and velocity metric can be realized together on a normalized complete flow with increasing precision, including noncommuting matrices. Hence a report has no larger optimal velocity risk on every complete flow *if and only if* it removes at least as much error in every direction, at every precision. Every failed Gaussian-affine quadratic comparison has a complete flow witness. This is a distribution-free geometric statement: only the injected noise must be Gaussian; the target has finite variance and target and report laws are otherwise arbitrary. The same geometry compares the actual errors of fitted predictors and gives a uniform preference criterion within a prescribed family of objectives.

Reviewers: please read the Reviewer Guidelines (iclr.cc/Conferences/2027/ReviewerGuidelines) and the AI Policy for Reviewers (iclr.cc/Conferences/2027/AIPolicyForReviewers). If you used AI to expand, edit, or polish your review, please provide the input text to the LLM. Better still, consider skipping the LLM and submitting your original text: we, and the authors, are much more interested in your unedited thoughts than in what an LLM has to say. AI-assisted or not, you are putting your name and reputation behind your review: LLM-generated falsehoods, hallucinations or misrepresentations are subject to disciplinary action, which may include desk-rejecting all papers you have authored.

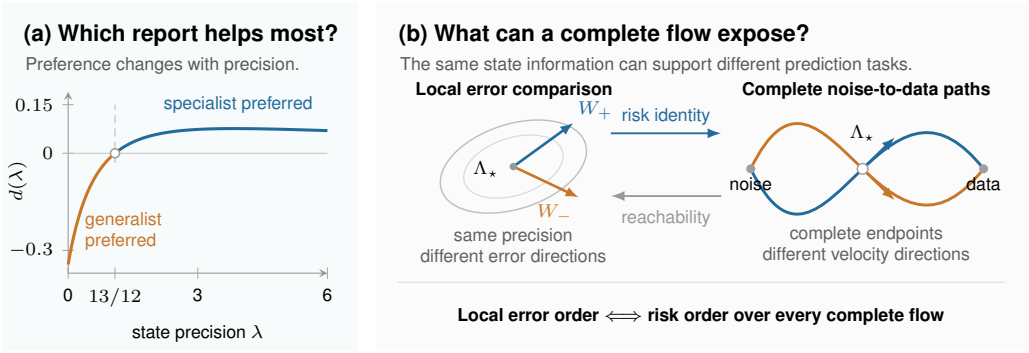


Figure 1: **Information value has precision and direction.** (a) The specialist–generalist difference in error removed, (1.1), changes sign at $13/12$. (b) A flow pairs the local error comparison with its velocity directions. Reachability supplies the converse: every positive precision–direction query occurs on a normalized complete path. The schematic paths meet at the same precision but test different directions, making the order exact.

Information value depends on what is already visible. For $H \sim \mathcal{N}(0, I_2)$, compare a specialist $S_A = 10H_1 + \varepsilon_A$ and a generalist $S_B = \sqrt{2}H + \varepsilon_B$, with independent standard Gaussian noises. After $Y_\lambda = \sqrt{\lambda}H + Z$, their difference in total posterior error reduction is

$$d(\lambda) = \frac{8(12\lambda - 13)}{(1+\lambda)(101+\lambda)(3+\lambda)}. \tag{1.1}$$

The generalist helps more below $13/12$, and the specialist above it (figure 1a). The matrix result identifies a second dependence: two complete flows with the same precision at every time can still read different error directions. Equivalent observations alone do not fix the flow's prediction objective.

From a complete order to a family decision. The complete order asks whether any flow can overturn a preference. A prescribed-family order asks whether it holds within a specified range. With precision history and clock fixed, a nonnegative worst contrast guarantees a common winner over the direction range; a negative one identifies a complete flow on which the preference changes.

From information order to fitted systems. The object of comparison is now the report together with its fitted predictor. Its actual error matrix retains information and fitting error. In a finite smooth direction span, one Gram matrix encodes every risk exactly. Conditional velocity regression on image and video targets tests the family decisions and selected risk differences on independent object sequences and videos.

2 Precision-indexed order and Euclidean reachability

The argument has one geometric step: complete flows can realize every local precision–direction query. Conditional projection then gives the information order; applying the same geometry to actual prediction errors gives the frozen-system order. The main objects have separate roles:

Object	Determined by	Meaning
H, X, S_a	Statistical experiment	Target, shared context and report
Λ_t, W_t	Coefficient path	State information and velocity error metric
$\mathsf{G}_{S_a}(\Lambda)$	Report and precision	Reduction of best achievable target error
$\mathsf{E}_a(\Lambda)$	Frozen system and precision	Actual target error, including fitting

Let $H \in L^2(\Omega; \mathbb{R}^d)$ and let X, S_a, S_b take values in standard-Borel spaces. Here X is shared context, S_a, S_b are reports, $Z \sim \mathcal{N}(0, I_d)$ is independent of them and H, and $v^{\otimes 2} = vv^\top$. Throughout, coefficients are fixed across contexts and reports, and predictors observe X. The report's error

reduction after a Gaussian query is

$$Y_\Lambda = \Lambda^{1/2} H + Z, \qquad \mathsf{G}_S(\Lambda) = \mathbb{E}[(\mathbb{E}(H \mid X, S, Y_\Lambda) - \mathbb{E}(H \mid X, Y_\Lambda))^{\otimes 2}].$$

Put $D_{ab}(\Lambda) = \mathsf{G}_{S_a}(\Lambda) - \mathsf{G}_{S_b}(\Lambda)$. Conditional Pythagoras gives

$$\mathsf{G}_S(\Lambda) = \mathsf{R}_X(\Lambda) - \mathsf{R}_{(X,S)}(\Lambda) \succeq 0,$$

where $\mathsf{R}_I(\Lambda) = \mathbb{E}\,\mathrm{Cov}(H \mid I, Y_\Lambda)$. These fields are continuous on the positive semidefinite cone (lemma A.1). No Gaussian assumption on H or the reports is used.

2.1 Euclidean flow risk and the complete order

An admissible Gaussian-affine path $F = (A_t, B_t)_{0 \le t \le 1}$ has absolutely continuous coefficients on $[0, 1]$, is C^1 in the interior, and satisfies

$$(A_0, B_0) = (I, 0), \qquad (A_1, B_1) = (0, I), \qquad A_t \text{ invertible for } t < 1,$$
$$\int_0^1 (\|\dot{A}_t\|_{\mathrm{F}}^2 + \|\dot{B}_t\|_{\mathrm{F}}^2)\, dt < \infty.$$

Thus the coefficients have their stated endpoint limits, and $Q_t = A_t Z + B_t H$ converges in L^2 to Z and H at the two ends. Its sample velocity $V_t = \dot{A}_t Z + \dot{B}_t H$ has finite action. For interior times define

$$R_t = A_t^{-1} B_t, \qquad \Lambda_t = R_t^\top R_t, \qquad K_t = A_t \dot{R}_t, \qquad W_t = K_t^\top K_t. \tag{2.1}$$

Differentiating $B_t = A_t R_t$ separates the observed drift:

$$V_t = \dot{A}_t A_t^{-1} Q_t + K_t H. \tag{2.2}$$

Whitening gives $A_t^{-1} Q_t = Z + R_t H$, whose informative coordinates are equivalent to Y_{Λ_t}. The observed drift cancels between reports; conditional projection of $K_t H$ gives their risk contrast. Writing $R_S^*(F) = \int_0^1 \mathbb{E}\|V_t - \mathbb{E}(V_t \mid Q_t, X, S)\|^2 dt$, we obtain

$$\Delta R_{ab}^*(F) := R_{S_b}^*(F) - R_{S_a}^*(F) = \int_0^1 \langle W_t, D_{ab}(\Lambda_t) \rangle_{\mathrm{F}}\, dt. \tag{2.3}$$

Positive values favor a. Each report's gain is bounded by the no-report velocity risk, so the integral is well defined. This is the standard conditional-projection step behind Gaussian MMSE comparison (Guo et al., 2005; Palomar & Verdú, 2006; Guo et al., 2011).

For the broader comparison, a *Gaussian-affine quadratic task* has linear observations and targets, jointly Gaussian noise independent of (H, X, S_a, S_b), nondegenerate observation noise, and a positive semidefinite quadratic loss. Its coefficients are fixed across reports and contexts. A predictor receives the observation, X and its report.

Theorem 2.1 (Complete Euclidean flow-risk order)**.** *The following are equivalent:*

- *(i)* $D_{ab}(\Lambda) \succeq 0$ *for every* $\Lambda \succ 0$*;*
- *(ii)* $\Delta R_{ab}^*(F) \ge 0$ *for every admissible path;*
- *(iii) the same inequality holds for every smooth admissible path with* $A_t A_t^\top + B_t B_t^\top = I$ *and* $\dot{\Lambda}_t \succ 0$ *in the interior.*
- *(iv) report* a *has no larger Bayes risk than* b *in every Gaussian-affine quadratic task.*

The field condition extends to $\Lambda \succeq 0$ *by continuity.*

Gaussian regression reduces each task in (iv) to a pairing $\langle \Gamma, D_{ab}(\Lambda) \rangle_{\mathrm{F}}$ with $\Gamma \succeq 0$; linear targets and Gaussian queries can read every such pair (proposition A.2). Thus (i) and (iv) express the same information order. Sufficiency for flows is (2.3). Necessity is the geometric inverse: precision and velocity direction must arise from the *same* complete coefficient path. This is why the flow test class is complete.

Theorem 2.2 (Euclidean reachability at a prescribed precision)**.** *For every interior $t_\star$ and every $\Lambda_\star, W_\star \succ 0$, there is a smooth endpoint-complete path, independent of the target and report laws, such that*

$$AA^\top + BB^\top = I, \quad \dot\Lambda_t \succ 0, \quad R_{t_\star} = \Lambda_\star^{1/2}, \quad W_{t_\star} = W_\star. \tag{2.4}$$

Its coefficient derivatives are bounded on $[0,1]$.

The construction separates precision from its orthogonal lift. At the requested point, put $P = \Lambda_\star^{1/2}$ and $Z = \{\Lambda_\star(I+\Lambda_\star)\}^{1/2}$. The positive matrix $G_\star = Z(Z^{-1}W_\star Z^{-1})^{1/2}Z$ and tangent $V_\star = P^{-1}G_\star$ satisfy

$$PV_\star = V_\star^\top P = G_\star \succ 0, \qquad V_\star^\top (I+\Lambda_\star)^{-1} V_\star = W_\star. \tag{2.5}$$

The first identity permits a strictly increasing precision curve with $\dot\Lambda_\star = 2G_\star$; the second realizes the requested velocity metric. Writing $R_t = O_t\Lambda_t^{1/2}$, an orthogonal factor supplies the skew part of the tangent without changing precision. This is the step that allows $\Lambda_\star$ and $W_\star$ to be noncommuting. The normalization $A = (I + RR^\top)^{-1/2}$, $B = AR$ and scalar cosine collars complete both endpoints (section A.2).

If the Loewner order fails, a positive direction detects that failure. Reachability embeds it at $t_\star$; continuity supplies a negative neighborhood; a smooth positive clock makes its integral negative. The witness remains normalized and strictly precision increasing. The theorem quantifies over the complete family with finite coefficient action; a prescribed range of changes has its own order below.

2.2 An exact counterpart for frozen predictors

The Bayes order concerns the information available from a report. A deployed system also has a specified fitted predictor. We now use its actual error in the same comparison. At $\Lambda \succ 0$, define canonical noise and signal coefficients C, T by

$$P = \Lambda^{1/2}, \quad C = (I+\Lambda)^{-1/2}, \quad T = PC, \quad M = T^2, \quad Q^{\mathrm{c}} = CZ^{\mathrm{c}} + TH, \tag{2.6}$$

where Z^{c} is standard Gaussian. For each report freeze $u_a(Q^{\mathrm{c}}, M, X, S_a)$, receiving neither path identity nor derivatives. Assume its coupled value is L^2 continuous in $\Lambda \succ 0$ and uniformly bounded in L^2 over that cone. Define

$$\begin{aligned} m_a &= TQ^{\mathrm{c}} + Cu_a, \qquad e_a = CH - TZ^{\mathrm{c}} - u_a, \\ \mathsf{E}_a(\Lambda) &= \mathbb{E}[(H-m_a)^{\otimes 2}] = C\mathbb{E}[e_a e_a^\top]C. \end{aligned} \tag{2.7}$$

The field includes the predictor's actual error and depends only on precision. To use it on a normalized path, take the polar factorization $R_t = O_t P_t$ and compute the observable input and velocity prediction

$$Q_t^{\mathrm{c}} = C_t O_t^\top A_t^{-1} Q_t, \qquad \widehat v_{a,F,t} = \dot A_t A_t^{-1} Q_t + K_t m_a. \tag{2.8}$$

Indeed, $O_t^\top Z$ is a standard carrier and the input has exactly the law in (2.6). Changing the orthogonal lift changes the velocity direction while reusing the same canonical predictor.

A diagonal reference path makes this interface familiar. Write $C = \mathrm{diag}(\cos\theta_i)$ and $T = \mathrm{diag}(\sin\theta_i)$. Its velocity output is $\mathrm{diag}(\dot\theta_i)u_a$. If $\dot\theta_i > 0$, coordinate rescaling converts any directly trained velocity predictor into this core, preserving its outputs and fitting errors on the reference precision curve (section A.5).

Theorem 2.3 (Complete order of frozen report–predictor systems)**.** *Let $\mathfrak{F}_+$ be the normalized admissible paths with R_t invertible for $0 < t < 1$. Their actual risks $\widehat R_a(F) = \int_0^1 \mathbb{E}\|V_t - \widehat v_{a,F,t}\|^2 dt$ are finite and*

$$\widehat R_b(F) - \widehat R_a(F) = \int_0^1 \langle W_t, \mathsf{E}_b(\Lambda_t) - \mathsf{E}_a(\Lambda_t)\rangle_{\mathrm{F}}\, dt, \tag{2.9}$$

$$\mathsf{E}_b(\Lambda) - \mathsf{E}_a(\Lambda) \succeq 0 \quad (\Lambda \succ 0) \iff \widehat R_b(F) \geq \widehat R_a(F) \quad (F \in \mathfrak{F}_+). \tag{2.10}$$

The equivalence still holds if paths are required to have $\dot\Lambda_t \succ 0$. Writing $m_a^* = \mathbb{E}(H \mid Q^{\mathrm{c}}, X, S_a)$,

$$\mathsf{E}_a(\Lambda) = \mathsf{R}_{(X,S_a)}(\Lambda) + \mathbb{E}[(m_a - m_a^*)^{\otimes 2}]. \tag{2.11}$$

The Bayes core satisfies the assumptions for every $H \in L^2$ and reduces the contrast field to D_{ab}.

The two orders coincide whenever the reports have equal fitting-error matrices; otherwise their difference gives the implementation's exact contribution to the comparison. The proof reuses the noncommuting witness of theorem 2.1. The stable residual $K_tC_te_a$, with $\|K_tC_t\|_{\mathrm{F}} \le \|\dot{B}_t\|_{\mathrm{F}} + \|\dot{A}_t\|_{\mathrm{F}}$, controls the complete integral (section A.5).

2.3 An exact order within prescribed changes of direction

Fix the entire precision curve $\Lambda_t = P_t^2 \succ 0$ and a continuous nonnegative profile ρ supported in a compact subinterval of $(0,1)$. The clock is fixed. Assume the canonical coefficients in (2.6) are smooth in the interior, absolutely continuous at the endpoints, and satisfy

$$(C_0,T_0) = (I,0), \quad (C_1,T_1) = (0,I), \qquad \mathcal{A}_0 = \int_0^1 (\|\dot{C}\|_{\mathrm{F}}^2 + \|\dot{T}\|_{\mathrm{F}}^2)dt < \infty.$$

For each smooth skew-symmetric Ω_t with $\|\Omega_t\|_{\mathrm{F}} \le \rho(t)$, solve $\dot{O} = O\Omega$, $O_0 = I$, and use

$$A_\Omega = CO^\top, \qquad B_\Omega = T. \tag{2.12}$$

This rotates the Gaussian carrier relative to the target. The state itself is canonical: $Q = C(O^\top Z) + TH$, with the same one-time law for every orientation. The terminal orientation need not return to I, because $C_1 = 0$ and $B_1 = I$. This removes a global constraint that would otherwise couple the allowed directions across time.

Put $\mathcal{E}_{ab}(t) = \mathbb{E}[e_be_b^\top - e_ae_a^\top]$; this is the same contrast in canonical residual coordinates, since $\mathsf{E}_b - \mathsf{E}_a = C\mathcal{E}_{ab}C$. Define

$$L_0 = \dot{T}C - \dot{C}T = C\dot{P}C, \qquad L_\Omega = L_0 + C\Omega T. \tag{2.13}$$

The canonical query law and frozen cores are unchanged by the orientation, so this residual contrast depends only on t. Define the lower envelope

$$\ell_\rho(t) = \min_{\substack{G^\top = -G \\ \|G\|_{\mathrm{F}} \le \rho(t)}} \left\langle (L_0 + CGT)^\top (L_0 + CGT), \mathcal{E}_{ab}(t) \right\rangle_{\mathrm{F}}. \tag{2.14}$$

Theorem 2.4 (Order under bounded changes of direction)**.** *The paths* (2.12) *are normalized, admissible, and have the prescribed precision Λ_t at every interior time. Their actual report risks satisfy*

$$\inf_{\substack{\Omega \text{ smooth},\ \Omega^\top = -\Omega \\ \|\Omega(t)\|_{\mathrm{F}} \le \rho(t)}} \{\widehat{R}_b(F_\Omega) - \widehat{R}_a(F_\Omega)\} = \int_0^1 \ell_\rho(t)dt. \tag{2.15}$$

Thus a is a common winner in this family exactly when the integral is nonnegative. A negative integral has a smooth strict witness in the same family. The same statements hold for Bayes risks using the Bayes cores. They also hold when both minimizations are restricted to any fixed linear subspace of skew matrices.

The speed profile bounds each allowed change before a report is chosen; it also bounds the rotation amplitude and coefficient action (equation (A.13)). If that curve is strictly precision increasing, every member remains so. Unlike the full-cone theorem, the criterion concerns only the prescribed curve and direction range.

The key identities are $A^{-1}B = OP$ and $V - \widehat{v}_a = L_\Omega e_a$. They turn a comparison of complete paths into the independent quadratic problems (2.14). Every normalized path with this precision has $A = UCO^\top$, $B = UT$ for an orthogonal U; its additional drift is observed and its residual $UL_\Omega e_a$ has the same Euclidean norm. Thus the representatives cover the directional comparisons within the prescribed rotation class, with their action bound for $U = I$. In skew coordinates, (2.14) is a classical trust-region problem (Moré & Sorensen, 1983). Section A.6 gives the global solution, including singular cases, and the smooth approximation establishing the exact infimum.

3 Consequences for report choice

A useful order beyond garbling. The flow order can decide between Blackwell-incomparable reports. For H uniform on $\{-1,0,1\}$, let A reveal $\mathbf{1}\{H = 1\}$ with probability $3/4$ and B reveal

$\mathbf{1}\{H = -1\}$ with probability $1/2$, using visible independent erasures otherwise. Neither report can be degraded into the other: each distinguishes two target values that the other treats identically. Yet reflection gives $G_A(\lambda) - G_B(\lambda) = g(\lambda)/4 > 0$ at every finite precision. Thus A has strictly smaller risk on every complete scalar flow (section A.4). The order concerns a specified target and family of prediction tasks, so it can resolve comparisons left open by an order over all decision problems.

Direction matters even at scalar precision. For $C = cI, T = sI$, where $c = \cos\theta$, $s = \sin\theta$, let $\mu_1 \le \mu_2$ be the two smallest eigenvalues of $\mathcal{E}_{ab}(t)$. In dimension $d \ge 2$, the local comparison has the closed form

$$\ell_\rho(t) = \dot\theta^2 \operatorname{tr} \mathcal{E}_{ab}(t) + \frac{c^2 s^2 \rho(t)^2}{2} \min\{\mu_1 + \mu_2, 0\}. \tag{3.1}$$

An allowed rotation reads a two-dimensional residual eigenspace. Above dimension two, this information is absent from the trace. The same state information can therefore produce different report choices; corollary A.5 gives an explicit construction with identical precision histories and equal coefficient action.

3.1 A CONTINUOUS FAMILY FROM A FINITE RISK MATRIX

The geometric order also gives an operational test for a declared family of changes. Fix smooth, compactly supported skew matrices $\Gamma_1(t), \dots, \Gamma_p(t)$ and let $\Omega_z(t) = \sum_j z_j \Gamma_j(t)$, with one global vector $z \in K_r := \{z : \|z\| \le r\}$. These controls define smooth complete paths by (2.12); matrices at different times may be noncommuting. With the induced speed envelope $\rho_r(t) = r \sup_{\|v\|\le 1} \|\sum_j v_j \Gamma_j(t)\|_F$, this is a finite-dimensional continuous subfamily of theorem 2.4. Write $L_j = C\Gamma_j T$ and $\mathcal{W}_a = [L_0 e_a, L_1 e_a, \dots, L_p e_a]$.

Proposition 3.1 (Exact risk coefficients). *If $\int \mathbb{E}\|\mathcal{W}_a\|_F^2 dt < \infty$, then the actual risk per target coordinate is*

$$\mathcal{R}_a(z) = x(z)^\top \mathsf{F}_a x(z), \qquad x(z) = (1, z^\top)^\top, \qquad \mathsf{F}_a = \frac{1}{d}\int_0^1 \mathbb{E}[\mathcal{W}_a^\top \mathcal{W}_a] dt \succeq 0. \tag{3.2}$$

These identities hold for every $z \in K_r$, without a continuity assumption on the core beyond measurability and integrability.

The residual is $\mathcal{W}_a x(z)$, and its canonical law is independent of z; squaring and integrating proves the result. This is an exact polynomial of population risks. Uniform random times and Gaussian carriers give unbiased observations of F_a directly from frozen predictor residuals. All observations from the same object or video are averaged into one independent unit before inference.

A margin for retaining a report. For a base-selected report a, define the worst challenger margin

$$m_{ab}(r) = \min_{z \in K_r} x(z)^\top (\mathsf{F}_b - \mathsf{F}_a) x(z). \tag{3.3}$$

Report a remains a winner throughout the family exactly when $m_{ab}(r) \ge 0$ for every challenger b. Each minimum is a classical trust-region problem, including indefinite and singular cases. The margins are continuous and nonincreasing in r. A negative margin identifies a smooth complete path on which retaining a has positive excess risk relative to b on that same path.

Uncertainty also transfers from the finite matrix to the whole family. If its paired estimation error is E, Cauchy–Schwarz bounds every risk error by $|E_{00}| + 2r\|E_{0+}\|_2 + r^2\|E_{++}\|_{\mathrm{op}}$. Paired natural-unit Gaussian multipliers calibrate these three blocks simultaneously across candidates and conditions, giving a uniform bound $\epsilon_{ab}(r)$ with asymptotic coverage $1 - \alpha$ under the moment and covariance conditions in section B. Consequently

$$m_{ab}(r) \in [\widehat{m}_{ab}(r) - \epsilon_{ab}(r), \widehat{m}_{ab}(r) + \epsilon_{ab}(r)] \tag{3.4}$$

holds even after report and path selection. Nonnegative lower bounds against every challenger certify reuse; a negative upper bound certifies failure. Otherwise the comparison remains unresolved.

Uniform preference separates report choice from objective choice. A system that passes the comparison can be selected before the final path in the declared family. A failed comparison identifies the objective on which selecting another system reduces velocity risk; independent paired losses test that difference after both choices are frozen. This is an order of prediction objectives along complete flows. Completeness also fixes the statistical destination: exact Bayes transport with a unique conditional flow solution reaches $\mathcal{L}(H \mid X, S)$ on every path (proposition A.6).

4 EXPERIMENTS

Does a preference measured on one velocity objective hold across a family of objectives? We study this question through conditional velocity regression on image and video targets. The candidates are fitted report–adapter–core systems, whose population velocity risks are ordered by theorem 2.3. The experiment tests a uniform decision: either one system remains preferable throughout the family, or the comparison identifies a flow on which another has lower risk. Independent natural samples then test the selected risk differences.

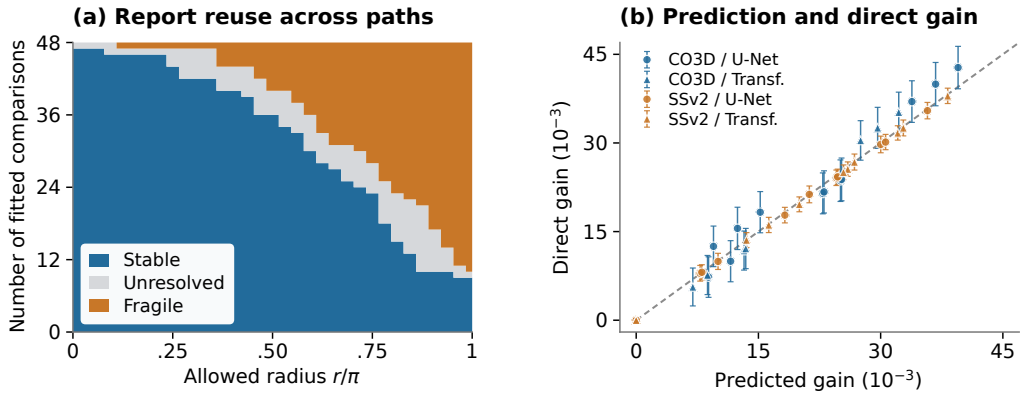


Figure 2: **Uniform preference and independent velocity-risk evidence.** (a) Family decisions for all 48 fit–curve comparisons at 33 allowed radii, using one simultaneous coefficient event. At $r = \pi$, 9 choices are stable, 38 are fragile and 1 is unresolved. (b) Predicted and independent direct gains from choosing again at all 48 selected tasks. Bars are simultaneous 95% direct intervals; 10 unchanged choices coincide at the origin. The dashed line is exact agreement.

CO3Dv2 supplies a novel-view target, two source views and camera context; SSv2 supplies a later-frame target and sixteen earlier source frames (Reizenstein et al., 2021; Goyal et al., 2017). Targets use the complete $16 \times 32 \times 32$ SD3.5 VAE latent. Image reports are CLIP, SigLIP 2 and DINOv3; video reports are CLIP, VideoMAE V2 and V-JEPA 2.1. Native spatial and temporal tokens are retained. A U-Net and a transformer each have four fits on disjoint training partitions, using the same source identities, context and objective for all reports. Their canonical cores receive noisy states and precision; the analytic wrapper supplies the path-dependent velocity in (2.8).

Which part of the preference comes from direction? The design-set channel covariance fixes four equal-rank target subspaces. Three smooth precision histories reveal them together (Scalar), in a sustained order (Separated), or with an ordering that changes during decoding (Crossing). At any fixed precision history, carrier orientation parameterizes the directional risk comparisons in theorem 2.4. We use all six orthonormal skew directions in the four-block space and two temporal modes, giving twelve global control coefficients. The primary family is $\|z\|_2 \leq \pi$; its smooth controls vanish near both endpoints and may be noncommuting across time. The normalized angular speed satisfies $\|\Omega_z(t)\|_F/\sqrt{d} \leq (\pi/2)b(t)$ for the fixed profile $0 \leq b \leq 1$. The primary family rotates the carrier by less than 0.64 radians in any plane throughout the path (equation (C.1)). Every member has the same joint law of noisy state, target, context and reports at each time, as well as the same clock and endpoints. Thus a changed preference identifies sensitivity to the velocity objective while the available input information remains fixed.

Each coefficient unit contributes a 13×13 risk Gram from 256 paired time/carrier records. One simultaneous event covers all report pairs, histories, fits and controls. We classify the base winner at $z = 0$ using (3.3), then freeze a fixed equal mixture of the twelve modes and the path with the most negative estimated margin. Independent direct units supply 256 fresh paired records to compare all reports on each identical task. Intervals are simultaneous 95% intervals within the coefficient and direct families, respectively. Section C gives full interfaces and individual-fit comparisons.

A single-objective winner can have a finite range of preference. Figure 2a shows how the decision evolves as the allowed direction range grows. At $r = \pi/2$, 36 choices certify reuse, 8 certify its failure, and 4 remain unresolved. At the primary radius, 9 of the 48 comparisons certify a common winner throughout the family, 38 certify failed reuse, and one remains unresolved. Both outcomes occur in image and video decoding. The stable lower margins range from 0.0021 to 0.0337 per coordinate; every fragile upper margin is below -0.0019. The decision curve quantifies a range of valid reuse; each negative margin identifies a task that falls outside that range.

Table 1: **Independent velocity risks of the frozen system choices.** Means average four fit-specific frozen choices. Retain/Choose are risks on the same selected witness; gains are in units of 10^{-3}, with simultaneous 95% half-widths. S/F/? counts stable/fragile/unresolved fits. Sc/Se/Cr denote Scalar/Separated/Crossing. Zero gain means the choices coincide.

Task / core	Curve	S/F/?	Retain	Choose	Witness gain	Fixed gain
CO3Dv2 / U-Net	Sc	0/4/0	1.160 ± 0.022	1.143 ± 0.021	16.696 ± 0.703	0
	Se	0/4/0	1.179 ± 0.022	1.152 ± 0.021	26.531 ± 0.868	0
	Cr	0/4/0	1.187 ± 0.022	1.162 ± 0.022	25.261 ± 0.929	0
CO3Dv2 / Transformer	Sc	2/1/1	1.179 ± 0.022	1.172 ± 0.022	7.607 ± 0.836	0
	Se	1/3/0	1.199 ± 0.022	1.186 ± 0.022	13.152 ± 0.953	0
	Cr	1/3/0	1.208 ± 0.023	1.195 ± 0.022	13.084 ± 1.011	0
SSv2 / U-Net	Sc	1/3/0	1.194 ± 0.008	1.178 ± 0.008	15.551 ± 0.366	0
	Se	1/3/0	1.207 ± 0.009	1.188 ± 0.008	18.792 ± 0.406	0
	Cr	0/4/0	1.209 ± 0.009	1.191 ± 0.008	17.865 ± 0.272	0
SSv2 / Transformer	Sc	1/3/0	1.227 ± 0.009	1.209 ± 0.008	17.573 ± 0.351	0
	Se	1/3/0	1.241 ± 0.009	1.220 ± 0.009	21.658 ± 0.391	1.218 ± 0.303
	Cr	1/3/0	1.240 ± 0.009	1.222 ± 0.009	17.988 ± 0.351	0

Selected risk differences persist on independent samples. All 38 report changes selected by the family comparison have positive direct gain intervals on 700 new object sequences and 4,811 new videos (figure 2b). Individual gains range from 0.0056 to 0.0428 per coordinate. The twelve task–core–history means all have positive lower gain bounds; their reductions are 0.64–2.25% of the risk incurred by retaining the original report (table 1). The fixed mixture changes one choice, also with a positive direct interval. A preference at one changed objective and a preference throughout the family are distinct statistical questions. The family minimum locates the objective that distinguishes them; independent paired losses confirm the corresponding risk difference. Together, the stable margins and direct comparisons support both outcomes of the decision: a uniform winner, or a verified change in preference within the same declared family.

5 Related work

Blackwell's comparison of experiments relates garbling to dominance across decision risks (Blackwell, 1951; 1953; Torgersen, 1991). Classical results also characterize linear normal experiments through information matrices and compare vector estimators under matrix loss (Hansen & Torgersen, 1974; Stępniak, 1997). Information–risk identities can incorporate restricted hypothesis classes (Williamson & Cranko, 2024). PROVER's precision-indexed matrix comes from conditional projection; its new geometric result makes complete flows a complete test of this quadratic order, including Blackwell-incomparable pairs.

Gaussian-channel identities connect scalar and vector MMSE to mutual-information derivatives (Guo et al., 2005; Palomar & Verdú, 2006). Conditioning reduces MMSE, with the positive-SNR equality

condition given by Guo et al. (2011, Proposition 11). Crossing results compare arbitrary inputs with Gaussian references under specified channel structures (Bustin et al., 2013). Reachability exposes every violated precision–direction comparison through Euclidean velocity risk on a complete path. Its frozen-system counterpart compares actual residuals, retaining fitting error.

Schedules, parameterizations and weighting shape diffusion objectives (Ho et al., 2020; Song et al., 2021; Karras et al., 2022). The continuous-time variational bound is schedule invariant (Kingma et al., 2021); Euclidean velocity risk depends on squared speed. Conditional velocity projection underlies flow matching, rectified flow and stochastic interpolants (Lipman et al., 2023; Liu et al., 2023; Albergo et al., 2025). Structured linear processes appear in blurring diffusion, generalized DDIM and system-embedded bridges (Hoogeboom & Salimans, 2023; Zhang et al., 2023; Sobieski et al., 2025). Lee et al. (2025) optimize multidimensional inference coefficients with a frozen field. Liu et al. (2026) connect anisotropic schedules to matrix-weighted velocity objectives; Scimeca et al. (2025) shape spectral noise. These works make the coefficient path part of the prediction problem. PROVER characterizes when the preference between reports is invariant to that choice, through a necessary and sufficient precision–metric order.

CLIP and SigLIP 2 learn image–text representations (Radford et al., 2021; Tschannen et al., 2025); DINOv3 uses visual self-distillation (Siméoni et al., 2026), VideoMAE V2 masked video reconstruction (Wang et al., 2023), and V-JEPA 2.1 predictive video learning (Mur-Labadia et al., 2026). We compare their source reports with a shared target space. Representation autoencoders instead encode the target itself as a generative latent (Zheng et al., 2026).

Quadratic optimization on a parameter ball is the classical trust-region problem (Moré & Sorensen, 1983). Gaussian multiplier methods supply simultaneous inference for paired vectors from independent units (Chernozhukov et al., 2013). Here one simultaneous coefficient event controls every path in a declared span, including a path selected from the same observations.

6 Conclusion

Complete flows test the Gaussian-affine quadratic information order: Euclidean reachability gives every failed precision–direction comparison a normalized noise-to-data witness. The same principle orders actual fitted systems and determines uniform preference within prescribed path families, connecting each failed family decision to a testable risk difference.

AI use statement

In this work, we used generative AI tools to assist with checking the correctness of mathematical arguments and proofs and with writing code. Additionally, we used these tools to improve the language and readability of the manuscript, search for relevant literature, and check references. We have manually reviewed the mathematical arguments and proofs, code, and references involved in this AI-assisted work. The authors take full responsibility for the final manuscript and its mathematical claims, proofs, code, and references, including all AI-assisted content.

References

Michael S. Albergo, Nicholas M. Boffi, and Eric Vanden-Eijnden. Stochastic interpolants: A unifying framework for flows and diffusions. *Journal of Machine Learning Research*, 26:209:1–209:80, 2025.

David Blackwell. Comparison of experiments. In *Proceedings of the Second Berkeley Symposium on Mathematical Statistics and Probability*, pp. 93–102. University of California Press, 1951. doi: 10.1525/9780520411586-009.

David Blackwell. Equivalent comparisons of experiments. *The Annals of Mathematical Statistics*, 24 (2):265–272, 1953. doi: 10.1214/aoms/1177729032.

Ronit Bustin, Miquel Payaró, Daniel P. Palomar, and Shlomo Shamai (Shitz). On MMSE crossing properties and implications in parallel vector Gaussian channels. *IEEE Transactions on Information Theory*, 59(2):818–844, 2013. doi: 10.1109/TIT.2012.2225405.

Victor Chernozhukov, Denis Chetverikov, and Kengo Kato. Gaussian approximations and multiplier bootstrap for maxima of sums of high-dimensional random vectors. *The Annals of Statistics*, 41(6): 2786–2819, 2013. doi: 10.1214/13-AOS1161.

Patrick Esser, Sumith Kulal, Andreas Blattmann, Rahim Entezari, Jonas Müller, Harry Saini, Yam Levi, Dominik Lorenz, Axel Sauer, Frederic Boesel, Dustin Podell, Tim Dockhorn, Zion English, and Robin Rombach. Scaling rectified flow transformers for high-resolution image synthesis. In *Proceedings of the 41st International Conference on Machine Learning*, volume 235 of *Proceedings of Machine Learning Research*, pp. 12606–12633, 2024.

Raghav Goyal, Samira Ebrahimi Kahou, Vincent Michalski, Joanna Materzynska, Susanne Westphal, Heuna Kim, Valentin Haenel, Ingo Fründ, Peter Yianilos, Moritz Mueller-Freitag, Florian Hoppe, Christian Thurau, Ingo Bax, and Roland Memisevic. The "Something Something" video database for learning and evaluating visual common sense. In *Proceedings of the IEEE International Conference on Computer Vision*, pp. 5843–5851, 2017. doi: 10.1109/ICCV.2017.622.

Dongning Guo, Shlomo Shamai, and Sergio Verdú. Mutual information and minimum mean-square error in Gaussian channels. *IEEE Transactions on Information Theory*, 51(4):1261–1282, 2005. doi: 10.1109/TIT.2005.844072.

Dongning Guo, Yihong Wu, Shlomo Shamai (Shitz), and Sergio Verdú. Estimation in Gaussian noise: Properties of the minimum mean-square error. *IEEE Transactions on Information Theory*, 57(4): 2371–2385, 2011. doi: 10.1109/TIT.2011.2111010.

Ole Håvard Hansen and Erik N. Torgersen. Comparison of linear normal experiments. *The Annals of Statistics*, 2(2):367–373, 1974. doi: 10.1214/aos/1176342672.

Jonathan Ho, Ajay Jain, and Pieter Abbeel. Denoising diffusion probabilistic models. In *Advances in Neural Information Processing Systems*, volume 33, pp. 6840–6851, 2020.

Emiel Hoogeboom and Tim Salimans. Blurring diffusion models. In *International Conference on Learning Representations*, 2023.

Tero Karras, Miika Aittala, Timo Aila, and Samuli Laine. Elucidating the design space of diffusion-based generative models. In *Advances in Neural Information Processing Systems*, volume 35, pp. 26565–26577, 2022. doi: 10.52202/068431-1926.

Diederik P. Kingma, Tim Salimans, Ben Poole, and Jonathan Ho. Variational diffusion models. In *Advances in Neural Information Processing Systems*, volume 34, pp. 21696–21707, 2021. URL https://proceedings.neurips.cc/paper/2021/hash/b578f2a52a0229873fefc2a4b06377fa-Abstract.html.

Dohoon Lee, Jaehyun Park, Hyunwoo J. Kim, and Kyogu Lee. Multidimensional adaptive coefficient for inference trajectory optimization in flow and diffusion. In *Proceedings of the 42nd International Conference on Machine Learning*, volume 267 of *Proceedings of Machine Learning Research*, pp. 33635–33654. PMLR, 2025.

Yaron Lipman, Ricky T. Q. Chen, Heli Ben-Hamu, Maximilian Nickel, and Matthew Le. Flow matching for generative modeling. In *International Conference on Learning Representations*, 2023.

Pengxi Liu, Zeyu Michael Li, and Xiang Cheng. Variational trajectory optimization of anisotropic diffusion schedules. *CoRR*, abs/2602.19512, 2026. doi: 10.48550/arXiv.2602.19512. URL https://arxiv.org/abs/2602.19512.

Xingchao Liu, Chengyue Gong, and Qiang Liu. Flow straight and fast: Learning to generate and transfer data with rectified flow. In *International Conference on Learning Representations*, 2023.

Jorge J. Moré and D. C. Sorensen. Computing a trust region step. *SIAM Journal on Scientific and Statistical Computing*, 4(3):553–572, 1983. doi: 10.1137/0904038.

Lorenzo Mur-Labadia, Matthew J. Muckley, Amir Bar, Mido Assran, Koustuv Sinha, Mike Rabbat, Yann LeCun, Nicolas Ballas, and Adrien Bardes. V-JEPA 2.1: Unlocking dense features in video self-supervised learning. *CoRR*, abs/2603.14482, 2026. doi: 10.48550/arXiv.2603.14482. URL https://arxiv.org/abs/2603.14482.

Daniel Pérez Palomar and Sergio Verdú. Gradient of mutual information in linear vector Gaussian channels. *IEEE Transactions on Information Theory*, 52(1):141–154, 2006. doi: 10.1109/TIT.2005.860424.

Alec Radford, Jong Wook Kim, Chris Hallacy, Aditya Ramesh, Gabriel Goh, Sandhini Agarwal, Girish Sastry, Amanda Askell, Pamela Mishkin, Jack Clark, Gretchen Krueger, and Ilya Sutskever. Learning transferable visual models from natural language supervision. In *Proceedings of the 38th International Conference on Machine Learning*, volume 139 of *Proceedings of Machine Learning Research*, pp. 8748–8763, 2021.

Jeremy Reizenstein, Roman Shapovalov, Philipp Henzler, Luca Sbordone, Patrick Labatut, and David Novotný. Common objects in 3D: Large-scale learning and evaluation of real-life 3D category reconstruction. In *Proceedings of the IEEE/CVF International Conference on Computer Vision*, pp. 10881–10891, 2021. doi: 10.1109/ICCV48922.2021.01072.

Luca Scimeca, Thomas Jiralerspong, Berton Earnshaw, Jason S. Hartford, and Yoshua Bengio. Learning what matters: Steering diffusion via spectrally anisotropic forward noise. *CoRR*, abs/2510.09660, 2025. doi: 10.48550/arXiv.2510.09660. URL https://arxiv.org/abs/2510.09660.

Oriane Siméoni, Huy V. Vo, Maximilian Seitzer, Federico Baldassarre, Maxime Oquab, Cijo Jose, Vasil Khalidov, Marc Szafraniec, Seung Eun Yi, Michaël Ramamonjisoa, Francisco Massa, Daniel Haziza, Luca Wehrstedt, Jianyuan Wang, Timothée Darcet, Théo Moutakanni, Leonel Sentana, Claire Roberts, Andrea Vedaldi, Jamie Tolan, John Brandt, Camille Couprie, Julien Mairal, Hervé Jégou, Patrick Labatut, and Piotr Bojanowski. DINOv3. *Transactions on Machine Learning Research*, 2026, 2026. URL https://openreview.net/forum?id=2NlGyqNjns.

Bartlomiej Sobieski, Matthew Tivnan, Yuang Wang, Siyeop Yoon, Pengfei Jin, Dufan Wu, Quanzheng Li, and Przemyslaw Biecek. System-embedded diffusion bridge models. In *Advances in Neural Information Processing Systems*, volume 38, pp. 17006–17043, 2025. doi: 10.52202/085713-0573.

Yang Song, Jascha Sohl-Dickstein, Diederik P. Kingma, Abhishek Kumar, Stefano Ermon, and Ben Poole. Score-based generative modeling through stochastic differential equations. In *International Conference on Learning Representations*, 2021.

Stability AI. Introducing stable diffusion 3.5. Official model release, 2024. URL https://stability.ai/news-updates/introducing-stable-diffusion-3-5.

Czesław Stępniak. Matrix loss in comparison of linear experiments. *Linear Algebra and its Applications*, 264:341–348, 1997. doi: 10.1016/S0024-3795(97)00019-0.

Erik N. Torgersen. *Comparison of Statistical Experiments*, volume 36 of *Encyclopedia of Mathematics and its Applications*. Cambridge University Press, 1991. doi: 10.1017/CBO9780511666353.

Michael Tschannen, Alexey A. Gritsenko, Xiao Wang, Muhammad Ferjad Naeem, Ibrahim Alabdulmohsin, Nikhil Parthasarathy, Talfan Evans, Lucas Beyer, Ye Xia, Basil Mustafa, Olivier J. Hénaff, Jeremiah Harmsen, Andreas Steiner, and Xiaohua Zhai. SigLIP 2: Multilingual vision-language encoders with improved semantic understanding, localization, and dense features. *CoRR*, abs/2502.14786, 2025. doi: 10.48550/arXiv.2502.14786. URL https://arxiv.org/abs/2502.14786.

Limin Wang, Bingkun Huang, Zhiyu Zhao, Zhan Tong, Yinan He, Yi Wang, Yali Wang, and Yu Qiao. VideoMAE V2: Scaling video masked autoencoders with dual masking. In *Proceedings of the IEEE/CVF Conference on Computer Vision and Pattern Recognition*, pp. 14549–14560, 2023. doi: 10.1109/CVPR52729.2023.01398.

Robert C. Williamson and Zac Cranko. Information processing equalities and the information-risk bridge. *Journal of Machine Learning Research*, 25:103:1–103:53, 2024.

Qinsheng Zhang, Molei Tao, and Yongxin Chen. gDDIM: Generalized denoising diffusion implicit models. In *International Conference on Learning Representations*, 2023.

Boyang Zheng, Nanye Ma, Shengbang Tong, and Saining Xie. Diffusion transformers with representation autoencoders. In *International Conference on Learning Representations*, volume 2026, pp. 35791–35820, 2026. URL https://proceedings.iclr.cc/paper_files/paper/2026/hash/3c4141c12660ad3625eb4ae845e0a6f9-Abstract-Conference.html.

A PROOFS OF THE RISK ORDER AND ITS CONSEQUENCES

A.1 POSTERIOR VERSIONS, CONTINUITY, AND THE RISK IDENTITY

Lemma A.1 (Field regularity)**.** *For $H \in L^2$ and standard-Borel X, S, the posterior means admit jointly measurable versions in the query and precision. The averaged field is continuous on $\{\Lambda \succeq 0\}$ and satisfies*

$$0 \preceq \mathsf{G}_S(\Lambda) \preceq \Sigma_X^0 := \mathbb{E}[(H - \mathbb{E}(H \mid X))^{\otimes 2}]. \tag{A.1}$$

Proof. For $I = X$ or (X, S) choose a regular conditional law $P_I(dh)$ of H. With φ_d the standard Gaussian density, define

$$p_I(y, \Lambda) = \int \varphi_d(y - \Lambda^{1/2}h) P_I(dh),$$
$$n_I(y, \Lambda) = \int h\varphi_d(y - \Lambda^{1/2}h) P_I(dh), \qquad m_I(y, \Lambda) = n_I(y, \Lambda)/p_I(y, \Lambda). \tag{A.2}$$

The positive denominator, kernel integration, and continuous square root give joint measurability. Conditional Pythagoras, with vanishing matrix cross terms, gives $\mathsf{G}_S = \mathsf{R}_X - \mathsf{R}_{(X,S)}$; projection onto X then yields (A.1).

For $\Lambda_n \to \Lambda$, Gaussian translation continuity and dominated convergence give total-variation convergence of the joint laws of (H, X, S, Y_{Λ_n}). For bounded targets, restrict predictors to the same bounded convex range, making Bayes squared risk continuous under this convergence. Otherwise truncate the *prediction target*, retaining the original query: L^2 contraction makes truncation error uniform in precision. Passing to the limit and polarizing proves matrix continuity. Conditioning this argument on X, dominated by (A.1), also gives continuous conditional fields on a common full-measure set. □

Consider $O = BH + \xi$, $T = EH + \zeta$, and loss $(T - f)^\top M(T - f)$, $M \succeq 0$. Let (ξ, ζ) be centered jointly Gaussian, independent of (H, X, S), with $\mathrm{Cov}(\xi) = \Sigma \succ 0$ and $\mathrm{Cov}(\zeta, \xi) = \Omega$. Gaussian regression and whitening give

$$\Lambda = B^\top \Sigma^{-1} B, \qquad J = E - \Omega\Sigma^{-1}B, \qquad \Gamma = J^\top M J. \tag{A.3}$$

Proposition A.2 (Gaussian-affine quadratic risk identity)**.** *If the target has finite second moment, the decrease in Bayes risk from adding S to (O, X) is exactly $\langle \Gamma, \mathsf{G}_S(\Lambda)\rangle_{\mathrm{F}}$. Consequently the Bayes risk under S_b minus that under S_a is $\langle \Gamma, D_{ab}(\Lambda)\rangle_{\mathrm{F}}$.*

The proof of theorem 2.1 below also shows equivalence to nonnegative contrast for every such record.

Proof of proposition A.2. Whitening gives $\Sigma^{-1/2}O = RH + N$, $R = \Sigma^{-1/2}B$, with standard Gaussian N. An SVD separates independent Gaussian ancillaries, leaving the informative coordinates of $Y_{R^\top R}$. Both queries give the same posterior law of H given X, with or without S.

Gaussian regression writes $\zeta = \Omega\Sigma^{-1}\xi + \varepsilon$ with ε independent of ξ and (H, X, S). Thus $T = \Omega\Sigma^{-1}O + JH + \varepsilon$, $J = E - \Omega\Sigma^{-1}B$. The observed term and residual-noise risk cancel between information sets; nested projection of JH gives the gain $\mathrm{tr}[J^\top M J\, \mathsf{G}_S(\Lambda)]$.

For a path, differentiating $B_t = A_t R_t$ gives (2.2). Whitening by A_t^{-1} then gives (2.3). Each gain is bounded by the no-report velocity risk; independence and centering of Z give

$$\int_0^1 \mathbb{E}\|V_t\|^2 dt = \int_0^1 \{\|\dot{A}_t\|_{\mathrm{F}}^2 + \mathbb{E}\|\dot{B}_t H\|^2\}\, dt \le \max\{1, \mathbb{E}\|H\|^2\} \int_0^1 (\|\dot{A}_t\|_{\mathrm{F}}^2 + \|\dot{B}_t\|_{\mathrm{F}}^2)\, dt.$$

This proves integrability; coefficient convergence supplies the endpoints. □

A.2 THE NONCOMMUTING EUCLIDEAN INVERSE

Lemma A.3 (Positive matrix completion)**.** *Let $Q \succ 0$ and prescribe compatible smooth positive-definite matrix functions on sufficiently small neighborhoods of finitely many sites of $[a, b]$, using one-sided neighborhoods at endpoints. After shrinking those neighborhoods, there is a smooth $G(t) \succ 0$ agreeing with the prescribed functions there and satisfying $\int_a^b G(t)dt = Q$.*

Proof. Merge coincident prescriptions and denote the remaining functions by g_i. Put $q_0 = \lambda_{\min}(Q)$ and choose $0 < \eta < q_0/\{4(b-a)\}$. Choose disjoint neighborhoods $U_i \Subset V_i$, smooth cutoffs $0 \le \chi_i \le 1$ supported in V_i and equal to one in U_i, and a nonempty interval J outside all V_i. Shrink the neighborhoods until $\sum_i \int_{V_i} \|g_i - \eta I\|_{\mathrm{op}} < q_0/4$. Then

$$G_0 = \eta I + \sum_i \chi_i (g_i - \eta I), \qquad E_0 = \int_a^b G_0$$

is positive definite and $\|E_0\|_{\mathrm{op}} < q_0/2$. For a nonnegative smooth unit-mass bump h supported in J, set $G = G_0 + h(Q - E_0)$. This is positive definite, preserves all prescribed neighborhoods, and has the required integral. □

Proof of theorem 2.2. Set

$$\begin{aligned} P_\star &= \Lambda_\star^{1/2}, & Z_\star &= \{\Lambda_\star(I+\Lambda_\star)\}^{1/2}, \\ G_\star &= Z_\star(Z_\star^{-1} W_\star Z_\star^{-1})^{1/2} Z_\star, & V_\star &= P_\star^{-1} G_\star. \end{aligned} \tag{A.4}$$

Positive square roots give

$$P_\star V_\star = V_\star^\top P_\star = G_\star, \qquad V_\star^\top (I+\Lambda_\star)^{-1} V_\star = W_\star. \tag{A.5}$$

The second identity follows from $G_\star Z_\star^{-2} G_\star = W_\star$.

Use scalar endpoint precision $\lambda_0(t) I = \tan^2(\pi t/2) I$. Choose $0 < t_L < t_\star < t_R < 1$ with $\lambda_0(t_L) I \prec \Lambda_\star \prec \lambda_0(t_R) I$. On $[t_L, t_\star]$, apply lemma A.3 with target integral $\{\Lambda_\star - \lambda_0(t_L) I\}/2$, protecting the scalar function $\dot\lambda_0(t) I/2$ near t_L and the constant $G_\star$ near $t_\star$. On $[t_\star, t_R]$, use integral $\{\lambda_0(t_R) I - \Lambda_\star\}/2$ and the corresponding endpoint prescriptions. The constant pieces agree near $t_\star$. Integrating $\dot\Lambda_t = 2G(t)$ and adding the collars gives a smooth curve with $\Lambda_{t_\star} = \Lambda_\star$, $\dot\Lambda_{t_\star} = 2G_\star$, and $\dot\Lambda_t \succ 0$.

Let $P_t = \Lambda_t^{1/2}$. Its symmetric derivative at the anchor solves $P_\star \dot P_\star + \dot P_\star P_\star = 2G_\star$. The matrix

$$\Omega_\star = (V_\star - \dot P_\star) P_\star^{-1} \tag{A.6}$$

is skew-symmetric: multiplying $\Omega_\star + \Omega_\star^\top$ on both sides by $P_\star$ reduces the claim to the preceding Sylvester equation and (A.5). Choose $f \in C_c^\infty((t_L, t_R))$ with $f(t_\star) = 0$ and $f'(t_\star) = 1$, and set

$$O_t = \exp\{f(t)\Omega_\star\}, \qquad R_t = O_t P_t.$$

Then $R_t^\top R_t = \Lambda_t$, while $R_{t_\star} = P_\star$ and $\dot R_{t_\star} = \Omega_\star P_\star + \dot P_\star = V_\star$. Finally define

$$A_t = (I + R_t R_t^\top)^{-1/2}, \qquad B_t = A_t R_t. \tag{A.7}$$

Thus $AA^\top + BB^\top = I$, and (A.5) gives $(A_{t_\star}\dot R_{t_\star})^\top (A_{t_\star}\dot R_{t_\star}) = W_\star$. On both scalar collars, $O_t = I$ and $(A_t, B_t) = (\cos(\pi t/2) I, \sin(\pi t/2) I)$. These collars and the smooth compact middle give bounded derivatives, finite action, and the stated endpoints. Only the query and anchor time enter the construction. □

A.3 Positive clocks and the complete order

Lemma A.4 (The change of clock)**.** *Let F be admissible and let ϕ be a smooth increasing bijection of $[0,1]$ with $\phi' > 0$. For $F_t^\phi = F_{\phi(t)}$,*

$$\Lambda_t^\phi = \Lambda_{\phi(t)}, \qquad W_t^\phi = \phi'(t)^2 W_{\phi(t)}.$$

If $q(s) = \langle W_s, D_{ab}(\Lambda_s)\rangle_{\mathrm{F}}$, then

$$\Delta R_{ab}^*(F^\phi) = \int_0^1 v(s) q(s) ds, \qquad v(s) = \phi'\{\phi^{-1}(s)\}, \qquad \int_0^1 v(s)^{-1} ds = 1. \tag{A.8}$$

The path remains admissible. Normalization and strict precision increase, when present, are preserved.

Proof. Differentiate and substitute $s = \phi(t)$. The positive continuous speed v and its reciprocal are bounded, so the new coefficient action is at most $\|v\|_\infty$ times the original action. Endpoints are unchanged, and $\dot{\Lambda}^{\phi}_t = \phi'(t)\dot{\Lambda}_{\phi(t)}$. □

Conversely, for smooth $w > 0$ set

$$c = \int_0^1 w(s)^{-1} ds, \qquad h(s) = c^{-1} \int_0^s w(r)^{-1} dr, \qquad \phi = h^{-1}. \tag{A.9}$$

Then $v = cw$ and $\Delta R^*_{ab}(F^\phi) = c \int wq$. If q is continuous and negative near an interior point, choose a nonnegative unit-mass bump ψ there. The legal clock from $w = (1-e)\psi + e$ has $\int wq < 0$ for sufficiently small $e > 0$.

Proof of theorem 2.1. Field dominance implies every path inequality by (2.3), so (i) implies (ii), which implies (iii). If (i) fails at $\Lambda_\star \succ 0$, cone self-duality supplies $W_0 \succeq 0$ with $\langle W_0, D_{ab}(\Lambda_\star)\rangle_{\mathrm{F}} < 0$. A sufficiently small identity ridge gives $W_\star = W_0 + \eta I \succ 0$ with the same strict sign. Theorem 2.2 realizes this query on a normalized, strictly precision-increasing path. Field regularity and smooth coefficients make the density continuous near the anchor. The clock above gives a strict negative contrast while preserving both properties, contradicting (iii).

Proposition A.2 proves (iv) from (i). Conversely the record $O = \Lambda_\star^{1/2} H + Z, T = W_\star^{1/2} H, M = I$ reads any strictly positive query, so (iv) implies (i). Continuity extends the field order to the boundary of the precision cone. Applying both orientations gives the corresponding equality statement. □

A.4 Strict field order for incomparable reports

For the erased indicators in section 3, the observed flag is independent of (H, Y_λ), so each gain is its reveal probability times the unerased gain. Reflection $(H, Y_\lambda) \mapsto (-H, -Y_\lambda)$ preserves the law and exchanges the indicators, making their unerased gains the same $g(\lambda)$.

At every finite λ and real $Y_\lambda = y$, all three target values have positive posterior mass. Given the positive indicator, the posterior mean is one; given its complement, it lies in $(-1, 0)$. Their positive conditional variance gives $g(\lambda) > 0$. At zero precision, $g(0) = \frac{1}{3}(1)^2 + \frac{2}{3}(-\frac{1}{2})^2 = \frac{1}{2}$. Consequently $G_A - G_B = g/4 > 0$, including the gap $1/8$ at zero. A complete scalar path has $K = A\dot{R} \neq 0$ on a set of positive measure; otherwise R is constant in the interior and cannot connect its endpoints. Integrating the strictly positive field gives a strictly positive risk gap.

Report A has identical conditional laws at $H = -1, 0$, while B distinguishes them; B has identical laws at $H = 0, 1$, while A distinguishes them. This rules out garbling in either direction. The incomparability persists even if the finite-precision Gaussian state is included in both experiments: the identical-report pair has mutually absolutely continuous joint observation laws, while the other report has a revealed-indicator event with positive probability at exactly one of those values. A Markov kernel preserves absolute continuity and cannot produce that event.

A.5 The full precision field of a frozen core

All expectations condition on fitted parameters, with one common evaluation law and independent canonical carrier. Write $U_a(\Lambda) = u_a(CZ^{\mathrm{c}} + TH, M, X, S_a)$ and $E_a(\Lambda) = CH - TZ^{\mathrm{c}} - U_a(\Lambda)$. The assumed uniform L^2 bound gives

$$\sup_{\Lambda \succ 0} \mathbb{E}\|E_a(\Lambda)\|^2 < \infty. \tag{A.10}$$

Interior L^2 continuity passes to $H - m_a = CE_a$, hence to E_a. Pointwise continuity with a common square-integrable envelope is a sufficient architecture-level condition.

Proof of theorem 2.3. For $F \in \mathfrak{F}_+$, polar decomposition $R = OP$ gives

$$CO^\top A^{-1} Q = CO^\top Z + CPH = CZ^{\mathrm{c}} + TH, \qquad Z^{\mathrm{c}} = O^\top Z.$$

Its joint law with (H, X, S_a, S_b) is the canonical law at this precision; this identifies one-time experiments, not carrier couplings across time. Because C, T commute and $C^2 + T^2 = I$,

$$H - m_a = CE_a, \qquad V - \widehat{v}_a = K(H - m_a) = KCE_a. \tag{A.11}$$

Using (2.2),

$$KC = (\dot{B} - \dot{A}R)C, \qquad \|KC\|_{\mathrm{F}} \le \|\dot{B}\|_{\mathrm{F}} + \|\dot{A}\|_{\mathrm{F}},$$

since $\|C\|_{\mathrm{op}} \le 1$ and $\|RC\|_{\mathrm{op}} = \|PC\|_{\mathrm{op}} \le 1$. The residual envelope and finite coefficient action prove finiteness and, by integration, (2.9). Endpoints are limits of these interior integrals.

Positive pairing gives sufficiency. For necessity, apply the proof of theorem 2.1 to the continuous field $\mathsf{E}_b - \mathsf{E}_a$: reachability realizes a strictly negative pairing on a neighborhood with $\dot{\Lambda} \succ 0$. A clock preserves the canonical query and core at each path location and multiplies its residual by the clock derivative. Thus (A.8) localizes the fitted density as well. The witness lies in $\mathfrak{F}_+$, proving also the increasing-precision variant without extending cores to singular interior precisions.

Conditional orthogonality in $H - m_a = (H - m_a^*) + (m_a^* - m_a)$ and equivalence of the canonical observation to Y_Λ give (2.11). For the Bayes core take $U_a^*(\Lambda) = \mathbb{E}(CH - TZ^{\mathrm{c}} \mid Q^{\mathrm{c}}, X, S_a)$. Conditioning $H = TQ^{\mathrm{c}} + C(CH - TZ^{\mathrm{c}})$ shows that its clean prediction is m_a^*. Conditional Jensen gives $\sup_\Lambda \mathbb{E}\|U_a^*(\Lambda)\|^2 \le \mathbb{E}\|H\|^2 + d$. On compact interior precision sets, the positive Gaussian posterior kernel gives L^2 continuity for a bounded target. Truncation of H and the L^2 contraction of conditional expectation extend this to m_a^*. Since C^{-1} is bounded on those sets, $U_a^* = C^{-1}(m_a^* - TQ^{\mathrm{c}})$ is locally L^2 continuous. Its fitting-error term vanishes, so $\mathsf{E}_b - \mathsf{E}_a = D_{ab}$. □

Direct velocity parameterization on a reference curve. On $A = C, B = T$, put $J_0 = \dot{C}C + \dot{T}T$ and $L_0 = \dot{T}C - \dot{C}T$. The inverse rotation of (Z^{c}, H) gives $V = J_0 Q^{\mathrm{c}} + L_0(CH - TZ^{\mathrm{c}})$. Wherever L_0 is invertible, a frozen direct predictor v_a^{ref} is represented exactly by $u_a = L_0^{-1}(v_a^{\mathrm{ref}} - J_0 Q^{\mathrm{c}})$. For diagonal angle curves, $J_0 = 0$ and $L_0 = \mathrm{diag}(\dot{\theta}_i)$. Strictly increasing angles identify time from precision, so the core is well defined on that curve. Changing its carrier orientation reuses this core and retains its actual error through $L_\Omega e_a$. An extension to other precisions is subject to the field assumptions of theorem 2.3.

A.6 The order on a fixed precision curve

Proof of theorem 2.4. The ODE $\dot{O} = O\Omega$, $O_0 = I$, gives $O^\top O = I$. For $A = CO^\top$, $B = T$,

$$AA^\top + BB^\top = C^2 + T^2 = I, \qquad A^{-1}B = OP, \qquad (A^{-1}B)^\top (A^{-1}B) = P^2.$$

The canonical coefficient endpoints give $(A_0, B_0) = (I, 0)$ and $(A_1, B_1) = (0, I)$ for every terminal O_1. Since Ω has compact interior support, O is constant on both endpoint neighborhoods. Thus the construction preserves endpoint regularity and requires no return of the orientation. For noncommuting Ω at different times the ODE, rather than an exponential of its integral, defines O.

Put $Z^{\mathrm{c}} = O^\top Z$ and $E_0 = CH - TZ^{\mathrm{c}}$. At every fixed time Z^{c} is standard Gaussian independent of the target and reports, and the actual state $Q = CZ^{\mathrm{c}} + TH$ has the canonical law. Since $(O^\top)' = -\Omega O^\top$,

$$V = (\dot{C} - C\Omega)Z^{\mathrm{c}} + \dot{T}H.$$

Substitute $Z^{\mathrm{c}} = CQ - TE_0$ and $H = TQ + CE_0$ to obtain

$$\begin{aligned} J_\Omega &= \dot{C}C + \dot{T}T - C\Omega C, \\ L_\Omega &= \dot{T}C - \dot{C}T + C\Omega T, \\ V &= J_\Omega Q + L_\Omega E_0, \qquad \widehat{v}_a = J_\Omega Q + L_\Omega u_a. \end{aligned} \tag{A.12}$$

Differentiating $T = CP$ gives $\dot{T}C - \dot{C}T = C\dot{P}C$: C and P commute, but $\dot{P}$ need not commute with either. Consequently $V - \widehat{v}_a = L_\Omega e_a$. This proves the risk identity underlying (2.15), including for noncommuting curves.

The coefficient action is finite, with

$$\mathcal{A}_{\mathrm{coeff}}(F_\Omega) = \int_0^1 \{\|\dot{C} - C\Omega\|_{\mathrm{F}}^2 + \|\dot{T}\|_{\mathrm{F}}^2\} dt \le (\sqrt{\mathcal{A}_0} + \|\rho\|_{L^2})^2. \tag{A.13}$$

The inequality is the triangle inequality in the L^2 space of matrix pairs and $\|C\|_{\mathrm{op}} \le 1$. If $C\dot{C} = \dot{C}C$, then $\left\langle \dot{C}, C\Omega \right\rangle_{\mathrm{F}} = 0$ by symmetry and skew-symmetry. In that case the action is exactly $\mathcal{A}_0 + \int \|C\Omega\|_{\mathrm{F}}^2$. Only Ω, not $\dot{\Omega}$, occurs in these derivatives. Moreover,

$$\|O_t - I\|_{\mathrm{F}} \le \int_0^t \|\Omega_s\|_{\mathrm{F}} ds, \qquad \sup_t \|A_\Omega - C\|_{\mathrm{F}} \le \|\rho\|_{L^1}.$$

The residual envelope in (A.10), $\|L_0\|_{\mathrm{F}} \le \|\dot{C}\|_{\mathrm{F}} + \|\dot{T}\|_{\mathrm{F}}$, and $\rho \in L^2$ prove risk integrability.

Every admissible direction has integrand at least ℓ_ρ, proving one inequality in (2.15). For the reverse inequality, let $\{G_j\}$ be a countable dense subset of the unit ball of skew matrices. Continuity in the direction variable gives

$$\ell_\rho(t) = \inf_j \left\langle (L_0 + C\rho G_j T)^\top (L_0 + C\rho G_j T), \mathcal{E}_{ab}(t) \right\rangle_{\mathrm{F}}.$$

This is measurable. For any $\epsilon > 0$, choose the first index whose value is at most $\ell_\rho(t) + \epsilon$. It gives a measurable unit-ball-valued $G(t)$ and a direction $\rho(t)G(t)$ whose integrated contrast is within ϵ of the lower envelope.

Extend G by zero and convolve with nonnegative smooth unit-mass mollifiers. Convexity preserves the unit-ball constraint and the smooth functions G_n approach G almost everywhere along a sequence. For smooth ρ, the directions ρG_n are already legal. For continuous ρ, take smooth compactly supported minorants $0 \le \rho_n \le \rho$ converging uniformly to ρ and use $\rho_n G_n$. Such minorants follow by smooth uniform approximation, subtraction of its error bound, and a smooth positive part from below. Their supports lie in $\{\rho > 0\}$. The uniform integrable bound

$$\|\mathcal{E}_{ab}(t)\|_{\mathrm{op}} (\|L_0(t)\|_{\mathrm{F}} + \rho(t))^2$$

allows dominated convergence. Smooth legal directions thus approach the measurable contrast, proving equality of the infima. A strict negative envelope leaves room for this approximation and yields a smooth strict witness. Equality does not require a smooth minimizing selector. For a fixed linear subspace of skew matrices, choose the dense set in its unit ball; convolution and scalar multiplication stay in that subspace, so the same proof applies. The Bayes core in theorem 2.3 gives the Bayes assertions. □

The normalization is compatible with every left output orientation. Indeed, a normalized path with $R = OP$ has $A = UCO^\top$, $B = UT$ for some orthogonal U; its canonical input is $U^\top Q$ and its residual multiplier is UL_Ω. Euclidean residual risk is unchanged by U. The representatives above take $U = I$, which supplies the endpoint completion and the action bound.

The pointwise quadratic certificate. Take a Frobenius orthonormal skew basis $\{J_i\}_{i=1}^{d(d-1)/2}$, write $\Omega = \sum_i z_i J_i$, and put $B_i = CJ_iT$. Then

$$\begin{aligned} q(t,z) &= c + 2b^\top z + z^\top \mathcal{H} z, \qquad \|z\| \le \rho(t), \\ c &= \left\langle L_0^\top L_0, \mathcal{E}_{ab} \right\rangle_{\mathrm{F}}, \quad b_i = \left\langle L_0^\top B_i, \mathcal{E}_{ab} \right\rangle_{\mathrm{F}}, \\ \mathcal{H}_{ij} &= \left\langle B_i^\top B_j, \mathcal{E}_{ab} \right\rangle_{\mathrm{F}}. \end{aligned} \tag{A.14}$$

The last matrix is symmetric by transposing the trace. For $\rho > 0$, a global minimizer has a multiplier λ satisfying

$$\begin{gathered} \mathcal{H} + \lambda I \succeq 0, \qquad (\mathcal{H} + \lambda I)z = -b, \qquad \lambda \ge 0, \quad \|z\| \le \rho, \\ \lambda(\|z\|^2 - \rho^2) = 0. \end{gathered} \tag{A.15}$$

These are the classical trust-region conditions (Moré & Sorensen, 1983). For completeness, they imply, for every feasible y,

$$q(t,y) - q(t,z) = (y-z)^\top (\mathcal{H} + \lambda I)(y-z) - \lambda(\|y\|^2 - \|z\|^2) \ge 0.$$

To find such a certificate, diagonalize $\mathcal{H}$ and set $\lambda_0 = \max\{0, -\lambda_{\min}(\mathcal{H})\}$. Above λ_0, the norm of $-(\mathcal{H} + \lambda I)^{-1} b$ decreases continuously to zero. A root with norm ρ supplies a boundary solution. A positive semidefinite unconstrained stationary point of norm at most ρ uses $\lambda = 0$. In the remaining

singular case, b is orthogonal to the lowest eigenspace and $z_0 = -(\mathcal{H} + \lambda_0 I)^\dagger b$ has norm below ρ. When $\lambda_0 > 0$, add a vector in $\ker(\mathcal{H} + \lambda_0 I)$ of norm $\sqrt{\rho^2 - \|z_0\|^2}$. The result satisfies (A.15); boundary equalities follow by the corresponding limit. This includes the hard case. The value is

$$\ell_\rho = c - \lambda\rho^2 - b^\top (\mathcal{H} + \lambda I)^\dagger b. \tag{A.16}$$

For $\rho = 0$, return c directly; in dimension one there is no skew variable. This reduction uses global quadratic certificates without assuming a positive semidefinite report contrast.

Closed form at scalar precision. When $C = cI$, $T = sI$ and $L_0 = \dot\theta I$, skew-symmetry gives $L_\Omega^\top L_\Omega = \dot\theta^2 I + c^2 s^2 \Omega^\top \Omega$. The real canonical form of a skew matrix supplies orthonormal pairs (u_j, v_j) and nonnegative σ_j such that

$$\Omega^\top \Omega = \sum_j \sigma_j^2 (u_j u_j^\top + v_j v_j^\top), \qquad \|\Omega\|_{\mathrm{F}}^2 = 2 \sum_j \sigma_j^2.$$

Every rank-two orthogonal projection has pairing with a symmetric matrix at least the sum of its two smallest eigenvalues: in an eigenbasis its diagonal weights lie in $[0, 1]$ and sum to two. Hence the minimum of $\langle \Omega^\top \Omega, \mathcal{E}_{ab} \rangle_{\mathrm{F}}$ is $\rho^2 \min\{\mu_1 + \mu_2, 0\}/2$. If the sum is negative, equality uses one plane spanned by its two smallest eigenvectors and $\sigma = \rho/\sqrt{2}$; otherwise $\Omega = 0$ attains it. This proves (3.1), including repeated eigenvalues, odd dimensions and $\rho = 0$. In dimension two the sum is the trace itself. For the complete reduced skew span $\Omega = \Omega_m \otimes I_r$, use $\overline{E}_{ij} = \mathrm{tr}(\mathcal{E}_{ab,ij})/r$ and $\|\Omega_m\|_{\mathrm{F}} \le \rho_{\mathrm{small}}$. The normalized risk is $m^{-1} \mathrm{tr}(L_m^\top L_m \overline{E})$, so the same formula applies to $\overline{E}$ and ρ_{small}, divided by m.

A.7 A REVERSAL AT AN IDENTICAL PRECISION HISTORY

Corollary A.5 (Same precision, opposite winners)**.** *There are two fixed Gaussian reports of $H \sim \mathcal{N}(0, I_2)$, with constant X, and smooth normalized complete paths $F_\pm$ with the same strictly increasing precision history and coefficient action, such that*

$$\mathrm{tr}\, \mathsf{R}_{S_a}(\Lambda_t) = \mathrm{tr}\, \mathsf{R}_{S_b}(\Lambda_t), \qquad \Delta R^*_{ab}(F_+) > 0 > \Delta R^*_{ab}(F_-). \tag{A.17}$$

The paths can be arbitrarily close in C^1 without changing their clock.

For two blocks of common rank r, let $\mathcal{U}$ be an isometry, $c_j = \cos\theta_j$, $s_j = \sin\theta_j$, and use $\Omega_\pm = \pm\omega \left(\begin{smallmatrix} 0 & -\mathcal{U} \\ \mathcal{U}^\top & 0 \end{smallmatrix}\right)$. Then

$$L_\pm = \begin{pmatrix} \dot\theta_1 I & \mp\omega c_1 s_2 \mathcal{U} \\ \pm\omega c_2 s_1 \mathcal{U}^\top & \dot\theta_2 I \end{pmatrix}. \tag{A.18}$$

The diagonal blocks of $L_\pm^\top L_\pm$ agree; their upper cross blocks are $\pm\omega k \mathcal{U}$, where $k = \dot\theta_2 c_2 s_1 - \dot\theta_1 c_1 s_2$. Contraction gives

$$\frac{\widehat{R}_a(F_-) - \widehat{R}_a(F_+)}{d} = -\frac{4}{d} \int_0^1 \omega k\, \mathbb{E}\langle e_{a,1}, \mathcal{U} e_{a,2} \rangle\, dt. \tag{A.19}$$

The direct representatives have common coefficient action

$$r \int \{\dot\theta_1^2 + \dot\theta_2^2 + \omega^2 (c_1^2 + c_2^2)\}\, dt.$$

Proof of corollary A.5. Let X be constant and take independent standard report noises in

$$S_a = K_+^{1/2} H + \xi_a, \quad S_b = K_-^{1/2} H + \xi_b, \qquad K_\pm = \begin{pmatrix} 2 & \pm 1 \\ \pm 1 & 2 \end{pmatrix}.$$

At $\Lambda = \mathrm{diag}(\lambda_1, \lambda_2)$, inversion of $I + \Lambda + K_\pm$ gives

$$D_{ab}(\Lambda) = \frac{2}{\mathcal{D}} \begin{pmatrix} 0 & 1 \\ 1 & 0 \end{pmatrix}, \qquad \mathcal{D} = (3 + \lambda_1)(3 + \lambda_2) - 1. \tag{A.20}$$

The posterior traces agree. Put $\alpha = \pi/2$ and choose a nonnegative smooth interior bump b equal to $b_0 > 0$ on an interval I. For $0 < \epsilon \|b'\|_\infty < \alpha$, set $\theta_{1,2} = \alpha t \pm \epsilon b(t)$ and $P = \mathrm{diag}(\tan\theta_1, \tan\theta_2)$.

Both angles increase strictly to their prescribed endpoints. Let $\omega = \delta f$ for a nonnegative smooth unit-mass function f supported in I, and use $\Omega_\pm = \pm\omega \left(\begin{smallmatrix} 0 & -1 \\ 1 & 0 \end{smallmatrix}\right)$ in (2.12). No compensating loop is needed.

The two paths share P^2 and have equal coefficient action. With $k = \dot\theta_2 c_2 s_1 - \dot\theta_1 c_1 s_2$, their W cross entries are $\pm\omega k/(c_1 c_2)$, so

$$\Delta R^*_{ab}(F_\pm) = \pm 4 \int \frac{\omega k}{\mathcal{D} c_1 c_2}\, dt. \tag{A.21}$$

On the support of f, $k = \alpha \sin(2\epsilon b_0) > 0$. The integral is strictly positive and finite. The coefficient and derivative bounds in section A.6 show that both paths approach the zero-direction path in C^1 as $\delta \downarrow 0$. □

This example also identifies a boundary of the restricted order. For a scalar two-dimensional precision, $C = cI$, $T = sI$ and $L_0 = \dot\theta I$. Every skew $\Omega = \omega \left(\begin{smallmatrix} 0 & -1 \\ 1 & 0 \end{smallmatrix}\right)$ satisfies

$$\left\langle L_\Omega^\top L_\Omega, \mathcal{E}_{ab} \right\rangle_{\mathrm{F}} = (\dot\theta^2 + c^2 s^2 \omega^2) \operatorname{tr} \mathcal{E}_{ab}.$$

The mirror reports have $\operatorname{tr} \mathcal{E}_{ab} = 0$, giving zero contrast for every allowed direction even though D_{ab} is indefinite. A fixed curve's constrained order therefore need not recover the full-cone order. This scalar calculation is specific to two dimensions.

A.8 The endpoint distribution

Proposition A.6 (Exact endpoint invariance)**.** *For every admissible path, the conditional interpolation laws solve the continuity equation driven by $v^*_{S,F,t}(q) = \mathbb{E}(V_t \mid Q_t = q, X, S)$. Whenever that equation has its unique flow solution on $t < 1$ from a Gaussian carrier independent of (H, X, S), its finite-energy endpoint satisfies*

$$\mathcal{L}(Q_1^* \mid X, S) = \mathcal{L}(H \mid X, S). \tag{A.22}$$

Every integrable endpoint loss against a target drawn independently given (X, S) has the same expectation for all such paths.

Proof. Condition on (X, S). The absolutely continuous chain rule gives, for every compactly supported smooth φ, the weak identity

$$\frac{d}{dt}\mathbb{E}[\varphi(Q_t) \mid X, S] = \mathbb{E}[\nabla\varphi(Q_t)^\top V_t \mid X, S] = \mathbb{E}[\nabla\varphi(Q_t)^\top v^*_{S,F,t}(Q_t) \mid X, S].$$

Conditional Jensen bounds this velocity's expected energy by the finite interpolation action. The coefficient endpoints give initial law $\mathcal{N}(0, I)$ and terminal limit $\mathcal{L}(H \mid X, S)$. Uniqueness identifies the flow marginals for $t < 1$. Almost every trajectory has finite energy, hence a Cauchy endpoint limit by Cauchy–Schwarz; its law is that terminal limit. The generated endpoint depends only on (X, S) and an initial carrier independent of the conditional target draw. Their joint conditional law is therefore the product of two copies of $\mathcal{L}(H \mid X, S)$, which determines every stated integrable endpoint loss. □

B Direct inference over a declared continuous family

All statements condition on the design transform, direction basis, report interfaces and trained cores. An independent unit is an entire object sequence or video; its repeated target, time and carrier records are averaged before inference. The coefficient and direct-evaluation units are disjoint. Risks refer to these frozen functions.

B.1 Exact coefficients from random-time residuals

For the family in section 3.1, define

$$\beta(t) = \sup_{\|v\| \le 1} \Big\| \sum_{j=1}^{p} v_j \Gamma_j(t) \Big\|_F.$$

It is continuous and compactly supported. Every control with $\|z\| \le r$ satisfies $\|\Omega_z(t)\|_F \le r\beta(t)$. The ODE $O_z' = O_z\Omega_z$, $O_z(0) = I$, therefore gives a smooth orthogonal lift and a complete normalized path $A_z = CO_z^\top$, $B_z = T$, with the fixed precision history. Its coefficient action is at most $(\sqrt{\mathcal{A}_0} + r\|\beta\|_{L^2})^2$ by (A.13). These statements allow arbitrary finite smooth skew bases, including time-noncommuting controls.

Proof of proposition 3.1. At each fixed time, $Z^{\mathrm{c}} = O_z^\top Z$ is standard Gaussian and independent of (H, X, S_a). Thus the canonical input and residual e_a have the same law for every z. The stable decomposition (A.12) gives $V_z - \widehat{v}_{a,z} = (L_0 + \sum_j z_j C\Gamma_j T)e_a = \mathcal{W}_a x(z)$. Squaring and integrating proves (3.2). The Gram is positive semidefinite, and the displayed integrability assumption makes every entry finite by Cauchy–Schwarz. No interpolation or continuity property of the core is used. □

Let stratum h have weight $\pi_h > 0$, $\sum_h \pi_h = 1$, and n_h independent coefficient units. For each unit draw L uniform times $T_{hi\ell}$ and independent canonical Gaussian carriers, paired across reports, curves and fits. Its coefficient observation is

$$Y_{hi,a} = \frac{1}{dL}\sum_{\ell=1}^{L} \mathcal{W}_a(T_{hi\ell})^\top \mathcal{W}_a(T_{hi\ell}), \qquad \widehat{\mathsf{F}}_a = \sum_h \frac{\pi_h}{n_h}\sum_i Y_{hi,a}. \tag{B.1}$$

Uniform random times integrate the full continuous-time objective: $\mathbb{E}_h Y_{hi,a} = \mathsf{F}_{h,a}$ and $\mathbb{E}\widehat{\mathsf{F}}_a = \mathsf{F}_a$ for the registered mixture. Finite L contributes to unit-score variance. The common canonical-noise coupling preserves the one-time marginal risks in the continuous integral.

For $p = 12$ the augmented matrix has 91 distinct entries. Let D_{hi} collect the upper-triangular entries of all paired matrices $Y_{hi,b} - Y_{hi,a}$ in the fixed comparison registry. Retain all within-unit covariance. Its mean and estimated covariance are

$$\widehat{\Delta} = \sum_h \frac{\pi_h}{n_h}\sum_i D_{hi}, \qquad \widehat{\Sigma} = \sum_h \frac{\pi_h^2}{n_h(n_h-1)}\sum_i (D_{hi} - \bar{D}_h)(D_{hi} - \bar{D}_h)^\top. \tag{B.2}$$

Independent tasks contribute separate covariance blocks.

B.2 One coefficient event for all radii and directions

For each paired matrix, use (B.2) to form the three scale estimates

$$s_0^2 = \widehat{\mathrm{Var}}(\widehat{F}_{00}), \quad s_1^2 = \sum_{j=1}^{p} \widehat{\mathrm{Var}}(\widehat{F}_{0j}), \quad s_2^2 = \sum_{i,j=1}^{p} \widehat{\mathrm{Var}}(\widehat{F}_{ij}), \tag{B.3}$$

where $\widehat{F} = \widehat{\mathsf{F}}_b - \widehat{\mathsf{F}}_a$. The last sum counts each off-diagonal entry twice. Draw independent $\xi_{hi} \sim N(0,1)$, shared across every coordinate of a unit, and set

$$Z^{\#} = \sum_h \frac{\pi_h}{n_h}\sqrt{\frac{n_h}{n_h - 1}}\sum_i \xi_{hi}(D_{hi} - \bar{D}_h). \tag{B.4}$$

Its conditional law is exactly $N(0, \widehat{\Sigma})$. Reshape each paired part into a symmetric matrix $E^{\#}$. The shared critical value $q_{1-\alpha}^{\#}$ is the conditional $(1-\alpha)$ quantile of

$$T^{\#} = \max_{\text{registered pairs and conditions}} \max\left\{ \frac{|E_{00}^{\#}|}{s_0}, \frac{\|E_{0+}^{\#}\|_2}{s_1}, \frac{\|E_{++}^{\#}\|_{\mathrm{op}}}{s_2} \right\}. \tag{B.5}$$

Exactly deterministic components are excluded from division and assigned zero error. In particular, under scalar precision every linear coefficient vanishes: L_0 is scalar and $C\Gamma_j T$ is skew, so $(L_0 e_a)^\top C\Gamma_j T e_a = 0$ for every record. A small observed variance alone does not justify declaring a component deterministic.

Proposition B.1 (Simultaneous continuous-family inference)**.** *Suppose the registry, coefficient dimension and strata are fixed and $n_h/n \to \rho_h > 0$. Units are mutually independent, including across strata and tasks, and identically distributed within each stratum, with a uniformly integrable*

$2+\delta$ moment envelope. Assume $n\widehat{\Sigma} \to_p \Sigma_\infty$ and $\sqrt{n}\, s_j \to_p \sigma_j > 0$ for each nonstructural component, and continuity of the limiting maximum distribution at its critical quantile. The matrix Σ_∞ may be singular. With probability at least $1-\alpha+o(1)$, for every registered pair and every $r \geq 0$,

$$\sup_{\|z\| \leq r} |\widehat{\Delta}_{ab}(z) - \Delta_{ab}(z)| \leq \epsilon_{ab}(r) := q^{\#}_{1-\alpha}(s_0 + 2r s_1 + r^2 s_2). \tag{B.6}$$

The event remains valid for reports, radii and controls selected from the coefficient sample within the declared comparison registry.

Proof. The stratified finite-dimensional central limit theorem and covariance consistency apply to (B.2). The Gaussian multiplier has the same joint limit; the continuous mapping theorem for the finite maximum of component norms, with consistent scales and the stated quantile condition, gives their joint confidence event (Chernozhukov et al., 2013). On this event the paired coefficient error satisfies $|E_{00}| \leq q s_0$, $\|E_{0+}\|_2 \leq q s_1$ and $\|E_{++}\|_{\mathrm{op}} \leq q s_2$. Expanding $x(z)^\top E x(z)$ and applying Cauchy–Schwarz proves (B.6) simultaneously for every r and z. There is no additional union over a continuum. □

The moment condition concerns quadratic coefficient observations. For bounded residual multipliers, residual $4+2\delta$ moments suffice.

For the finite multiplier simulation, allocate δ_{MC} of the error probability to critical-value simulation. From B independent draws use order statistic k, where

$$k = \min\{j \leq B : \Pr[\mathrm{Bin}(B, 1-\alpha+\delta_{\mathrm{MC}}) \geq j] \leq \delta_{\mathrm{MC}}\}. \tag{B.7}$$

Provided this set is nonempty, the simulated critical value is at least the conditional $(1-\alpha+\delta_{\mathrm{MC}})$ quantile except with probability δ_{MC}. The total error remains at most $\alpha + o(1)$. We use $B = 4999$ and $\delta_{\mathrm{MC}} = 0.001$ for the coefficient and direct critical values.

B.3 Margins, numerical extrema and independent decisions

The exact estimated quadratic minimum is a trust-region problem covered by (A.15), including its singular hard case. A uniform polynomial error transfers to its minimum and maximum. If numerical verification supplies a bracket $[\widehat{m}_L, \widehat{m}_U]$ for the estimated minimum, the population minimum lies in

$$[\widehat{m}_L - \epsilon_{ab}(r),\ \widehat{m}_U + \epsilon_{ab}(r)] \tag{B.8}$$

on the same event. Feasibility, stationarity, shifted-matrix positivity and primal–dual error are checked independently. A selected explicit control can instead be checked through its own feasible value and error bound. A negative upper minimum certifies failed reuse; a two-sided reversal additionally needs a positive lower base contrast for the same pair. Equation (B.8) propagates uncertainty through the exact quadratic minimum.

Freeze the base-selected report $\widehat{a}_0$, selected controls z_q and selected reports $\widehat{a}_q$ before opening the independent direct units. Their paired reuse gain is

$$I_q = \mathcal{R}_{\widehat{a}_0}(z_q) - \mathcal{R}_{\widehat{a}_q}(z_q). \tag{B.9}$$

Both terms use the same changed decoder. Construct a direct unit vector of all absolute risks, pairwise contrasts, reuse gains and candidate regrets. Formulae (B.2)–(B.4) apply to this vector. A shared studentized absolute-coordinate maximum gives simultaneous intervals

$$\widehat{\Delta}_j \ \pm\ q_{\mathrm{direct}} \sqrt{\widehat{\Sigma}_{jj}}. \tag{B.10}$$

Its conditions are the same within-stratum identical distribution and between-unit independence assumptions, applied to the direct scores: a $2+\delta$ moment envelope, $n_{\mathrm{direct}}\widehat{\Sigma}_{\mathrm{direct}} \to_p \Sigma_{\mathrm{direct},\infty}$, positive limiting $\sqrt{n_{\mathrm{direct}}}$-scaled standard errors on nonstructural coordinates, and a continuous limiting critical quantile. Deterministic self-comparisons have interval $[0,0]$. A positive lower gain endpoint confirms benefit; a negative upper endpoint confirms harm. If $U_{q,a}$ is the simultaneous upper endpoint for $\mathcal{R}_{\widehat{a}_q}(z_q) - \mathcal{R}_a(z_q)$, then $\mathcal{R}_{\widehat{a}_q}(z_q) - \min_a \mathcal{R}_a(z_q) \leq \max_a (U_{q,a})_+$ on this event. Repeated records remain clustered. The fixed four-fit mean is a linear average within each direct unit, so its covariance retains dependence between fits and its interval describes those four frozen functions. Fit-wise results remain separately visible. For displayed policy risk levels, averaging the four individual risk intervals gives a simultaneous interval for their mean. Gain intervals use the paired four-fit unit average directly.

C EXPERIMENTAL PROTOCOL

All squared losses are per target coordinate. Source identities, target transforms and decoder families freeze before fitting. Coefficient units select reports and queries; separate direct units evaluate those frozen choices. Section B specifies the simultaneous coefficient and direct intervals, including their assumptions and multiplier calibration.

C.1 OBSERVATIONS AND DISJOINT ROLES

CO3Dv2 uses object sequences from the released training partition (Reizenstein et al., 2021). Sort valid frames by released index: the target is nearest the median, and two distinct sources are nearest the first and third quartiles, with lower-index ties. Require usable cameras and a nonempty source object mask. Context contains source-to-target rigid transforms, source intrinsics and target-camera rays. Express translations in the target-camera frame and rotations in row order; apply the target crop/resize map to its intrinsics before computing normalized $K^{-1}(x, y, 1)^\top$ at latent-cell centers. Context and reports exclude target pixels and target-derived features.

SSv2 uses whole training videos (Goyal et al., 2017). For N ordered valid frames let $m = \lfloor (N - 1)/2 \rfloor$. Sources have indices $\lfloor jm/15 \rfloor, j = 0, \ldots, 15$, and the target has index $\lfloor 3(N-1)/4 \rfloor$. Require $m \geq 15$, sixteen distinct sources and a later target. Context contains source-to-target offsets divided by $N - 1$; action labels define strata only. Every report sees the same frames.

Within category/action strata, permute sorted eligible IDs using PCG64 seed 260928401, retain at most 100 sequences or 200 videos, and exclude strata with fewer than sixteen retained units. Cycle through seven roles: design, training I–IV, coefficient and direct. Derived records inherit their natural unit's role. In each training stratum reserve its final $\lceil n_h/5 \rceil$ units for stopping. Retained strata receive equal weight, and units equal weight within each stratum. Four-fit summaries condition on the four displayed functions and retain covariance from shared evaluation units.

Table 2: **Disjoint natural units.** Training counts include 153 stopping sequences per CO3Dv2 partition and 1,044 stopping videos per SSv2 partition. The common target RMS uses design units only.

Task	Strata	Design	Training partition				Coeff.	Direct	RMS
			I	II	III	IV			
CO3Dv2	51	750	749	708	708	706	705	700	0.9961
SSv2	174	4,978	4,972	4,962	4,955	4,829	4,821	4,811	1.0079

C.2 TARGET, REPORTS AND TRAINING

Center-crop RGB targets to their largest square and bicubically resize to 256^2. The frozen `stabilityai/stable-diffusion-3.5-large` VAE takes $[-1, 1]$ input; its posterior mode z gives $H_{\mathrm{raw}} = 1.5305(z - 0.0609) \in \mathbb{R}^{16\times32\times32}$ (Esser et al., 2024; Stability AI, 2024). Divide by the taskwise design RMS shared across reports, retaining all $d = 16384$ coordinates.

Image reports use `openai/clip-vit-large-patch14-336`, `google/siglip2-so400m-patch14-384` and `facebook/dinov3-vitl16-pretrain-lvd1689m` (Radford et al., 2021; Tschannen et al., 2025; Siméoni et al., 2026). Use official RGB normalization at 336^2, 384^2 and explicitly 256^2. CLIP vision last-hidden patch states exclude CLS and global projection; SigLIP2 retains the vision sequence before attention pooling; DINOv3 uses `x_norm_patchtokens`, excluding CLS and four register tokens. Their interfaces are 576×1024, 729×1152 and 256×1024 per image. Concatenate ordered sources. Video CLIP retains all sixteen framewise sequences. The self-supervised `OpenGVLab/VideoMAEv2-Large` uses sixteen 224^2 frames and 1568×1024 final-block states, extracted before the default `forward_features` mean pooling and `fc_norm` (Wang et al., 2023). Official `vjepa2_1_vit_large_384` uses distilled Large `ema_encoder` weights and explicit `num_frames=16`. Take the returned encoder in evaluation mode without

masks, discard its predictor, and retain 4608×1024 tokens from sixteen 384^2 frames (Mur-Labadia et al., 2026).

Encoders stay in evaluation mode. Tokenwise LayerNorm and a learned linear map project width to 256. A two-layer SiLU embedding adds patch centers, actual time offsets and source identity; all valid tokens enter cross-attention, ignoring masked padding. The adapter trains with its core. The U-Net has widths $128, 256, 384, 512$, two 3×3 residual blocks per stage, 32-group GroupNorm, SiLU, factor-two resampling, self-attention at 8^2, and eight-head report attention at 16^2 and 8^2. The transformer has 2×2 latent patches, width 512, eight blocks and heads, pre-LayerNorm, width-2048 SiLU feed-forward layers and report attention in every block. Both receive canonical noisy latents, four sine/cosine angle maps and context, with modulation scales $1 + \tanh a$ and shifts $\tanh b$.

Each core predicts $CH - Tz_c$ from $q_c = Cz_c + TH$, $z_c \sim N(0, I)$. Training samples four independent uniform angles in $[0, \pi/2]^4$ and minimizes squared residual per coordinate. Rotation, direction and angular speed are absent from the inputs. AdamW uses learning rate $2\,10^{-4}$, weight decay 10^{-4}, betas $(.9, .999)$, stabilizer 10^{-8}, batch 64 and gradient cap one. Initialization is Xavier-uniform, with zero biases, unit normalization scales and no dropout. Eight fixed angle/carrier records per stopping unit choose the checkpoint; stop after ten epochs without improvement or at 100 epochs, resolving ties toward the earlier checkpoint. Each disjoint partition supplies a fresh fit per core, with independent initialization streams. No fitting uses coefficient or direct units.

C.3 Complete paths in a twelve-parameter family

The centered design-set 16×16 channel covariance fixes an orthogonal basis. Order eigenvectors by decreasing eigenvalue, choosing the largest-magnitude coordinate positive with index ties. In repeated eigenspaces use Gram–Schmidt on projected coordinate vectors in index order. Four consecutive groups of four channels retain every spatial cell, each with rank 4096; group isometries pair local channels at the same cell. For $a = (-1, -1/3, 1/3, 1)$ and $\alpha = 1/4$, use

$$\theta_j^{\mathrm{sc}}(t) = \tfrac{\pi}{2} t, \qquad \theta_j^{\mathrm{sep}}(t) = \tfrac{\pi}{2}[t + \alpha a_j t(1-t)], \qquad \theta_j^{\mathrm{cross}}(t) = \tfrac{\pi}{2}[t + \alpha a_j \sin(2\pi t)/(2\pi)].$$

These curves are strictly increasing. Write $C_4 = \mathrm{diag}(\cos\theta_j)$, $T_4 = \mathrm{diag}(\sin\theta_j)$ and $D_4 = \mathrm{diag}(\dot\theta_j)$, extending each by $\otimes I_{4096}$. For $x = (t - 1/8)/(3/4)$ set $b(t) = \exp(4 - 1/[x(1-x)])$ on $0 < x < 1$ and zero elsewhere. Order $J_{ij} = (e_i e_j^\top - e_j e_i^\top)/\sqrt{2}$ as $(12, 13, 14, 23, 24, 34)$. A single global vector $z = (z^{\cos}, z^{\sin}) \in \mathbb{R}^{12}$ defines

$$\Omega_{4,z}(t) = b(t) \sum_{j=1}^{6} [z_j^{\cos} \cos(\pi t) + z_j^{\sin} \sin(\pi t)] J_j, \qquad \Omega_z = \Omega_{4,z} \otimes I_{4096}, \quad \|z\|_2 \le r.$$

The primary radius is $r = \pi$; nested families use $0 \le r \le \pi$. Since $\|\Omega_{4,z}\|_F \le b(t) r$, every member respects the same speed bound. Solve $O' = O\Omega_z$, $O(0) = I$, and take $A = CO^\top$, $B = T$. All paths share the entire precision curve and clock. Endpoint orientation is unrestricted because $C(1) = 0$ and $B(1) = I$. The two temporal modes allow noncommuting directions; the comparison covers the whole parameter ball.

The radius has a geometric interpretation independent of the reports. Let $O'_{4,z} = O_{4,z}\Omega_{4,z}$, $O_{4,z}(0) = I$, and let $\vartheta(O)$ be the largest principal rotation angle of O. The operator norm of a real skew matrix is at most its Frobenius norm divided by $\sqrt{2}$, since nonzero singular values occur in pairs. Hence

$$\sup_t \vartheta(O_{4,z}(t)) \le \int_0^1 \|\Omega_{4,z}(t)\|_{\mathrm{op}} dt \le \frac{r}{\sqrt{2}} \int_0^1 b(t) dt < 0.64 \qquad (r \le \pi). \tag{C.1}$$

The first inequality follows by integrating the angular speed of a unit vector in a principal rotation plane. Here $0.2878629479968 < \int b < 0.2878629479970$. The same bound holds at every intermediate time and under $O_z = O_{4,z} \otimes I_{4096}$. Thus r controls an explicit range of state-law-preserving rotations; the nested-radius comparison measures how much of this range preserves a report choice.

C.4 Coefficient queries and independent direct evaluation

For each frozen system write its velocity residual as $v_0 + \sum_{j=1}^{12} z_j v_j$, where $v_0 = L_0 e$ and $v_j = C\Gamma_j T e$ for the declared modes Γ_j. Each coefficient unit averages the per-coordinate 13×13 Gram

of these residual vectors over 256 paired uniform-time/Gaussian-carrier records. Its expectation is the exact continuous-time risk polynomial; there is no temporal interpolation. Streams for coefficient and direct records use seeds 260928411 and 260928413, respectively, with pairing across reports, curves and fits.

In each of the 48 task–core–fit–curve conditions, choose the smallest estimated identity risk among all three reports. Against that report, minimize each challenger's quadratic over $\|z\|_2 \le \pi$, handling singular trust-region cases. The most negative minimum selects the reuse witness; choose the minimum-risk report on that same path from all three candidates. Report ties use index; tied witness minima use control norm, then challenger index, with a fixed coordinate convention for singular solutions. Retain identity $z = 0$, the fixed query $z = \pi(1, \dots, 1)/\sqrt{12}$, and the reuse witness, including unchanged choices. Reports and queries freeze before direct units supply 256 fresh paired records each. Physical carriers are $Z = O(t)z_c$ and $V = A'Z + B'H$; this single-time coupling is not differentiated.

The coefficient event simultaneously covers all pairs, curves, cores and fits, including fixed four-fit means. Stable, fragile and unresolved classifications use the minimum-margin band; strict reversal additionally requires a positive identity-gap lower endpoint for the same pair. Direct gain compares retaining the identity-selected report with choosing again on the identical query. The multiplier procedures use 4999 draws and seeds 260928420 and 260928421, with the finite-draw quantile rule in section B. All absolute risks, paired intervals, fixed-query outcomes and individual-fit classifications are retained.

C.5 Complete family decisions

Table 3 gives every fit–curve comparison at the primary radius. The base report is the identity-risk minimizer from the coefficient sample. Its family margin is the minimum over both challengers and all controls in the ball. For challenger intervals $[L_b, U_b]$, the common event gives the margin interval $[\min_b L_b, \min_b U_b]$. A stable choice has a nonnegative lower endpoint; a fragile choice has a negative upper endpoint. These are statements about the complete parameter family.

Table 3: **All 48 family comparisons at $r = \pi$.** Margins and simultaneous 95% intervals are in units of 10^{-3}. U/T denote the U-Net and transformer; I–IV the fit; Sc/Se/Cr the precision history. Choices are identity/fixed/witness indices: 0 is CLIP; 1 and 2 are SigLIP2/DINOv3 for images and VideoMAEv2/V-JEPA2.1 for videos. S, F and ? mean stable, fragile and unresolved.

	CO3Dv2			SSv2		
Condition	Choice	Margin [interval]		Choice	Margin [interval]	
U-I-Sc	1/1/2	$-11.586\ [-16.472, -6.700]$	F	2/2/1	$-24.564\ [-26.315, -22.813]$	F
U-I-Se	1/1/2	$-25.069\ [-30.406, -19.732]$	F	2/2/1	$-30.011\ [-31.987, -28.036]$	F
U-I-Cr	1/1/2	$-25.203\ [-30.734, -19.673]$	F	2/2/1	$-18.244\ [-20.273, -16.215]$	F
U-II-Sc	2/2/1	$-33.837\ [-38.610, -29.063]$	F	1/1/2	$-7.852\ [-9.642, -6.062]$	F
U-II-Se	2/2/1	$-39.503\ [-44.729, -34.277]$	F	1/1/2	$-10.045\ [-12.115, -7.976]$	F
U-II-Cr	2/2/1	$-36.745\ [-42.170, -31.320]$	F	1/1/2	$-21.248\ [-23.303, -19.193]$	F
U-III-Sc	1/1/2	$-8.881\ [-13.719, -4.043]$	F	2/2/1	$-30.608\ [-32.331, -28.885]$	F
U-III-Se	1/1/2	$-22.901\ [-28.182, -17.619]$	F	2/2/1	$-35.745\ [-37.685, -33.805]$	F
U-III-Cr	1/1/2	$-23.049\ [-28.523, -17.575]$	F	2/2/1	$-24.724\ [-26.710, -22.738]$	F
U-IV-Sc	2/2/1	$-9.485\ [-14.388, -4.583]$	F	1/1/1	$5.968\ [4.321, 7.614]$	S
U-IV-Se	2/2/1	$-15.221\ [-20.591, -9.852]$	F	1/1/1	$4.251\ [2.323, 6.178]$	S
U-IV-Cr	2/2/1	$-12.432\ [-18.018, -6.845]$	F	1/1/2	$-8.058\ [-9.950, -6.165]$	F
T-I-Sc	2/2/1	$-27.540\ [-32.171, -22.909]$	F	1/1/2	$-13.538\ [-15.251, -11.826]$	F
T-I-Se	2/2/1	$-32.221\ [-37.290, -27.152]$	F	1/1/2	$-16.270\ [-18.248, -14.291]$	F
T-I-Cr	2/2/1	$-29.633\ [-34.902, -24.364]$	F	1/1/2	$-26.787\ [-28.762, -24.811]$	F
T-II-Sc	1/1/1	$1.232\ [-3.441, 5.905]$	?	2/2/1	$-32.099\ [-33.697, -30.502]$	F
T-II-Se	1/1/2	$-13.236\ [-18.355, -8.118]$	F	2/1/1	$-38.230\ [-40.028, -36.433]$	F
T-II-Cr	1/1/2	$-13.446\ [-18.752, -8.141]$	F	2/2/1	$-25.967\ [-27.804, -24.131]$	F
T-III-Sc	2/2/2	$19.334\ [14.751, 23.917]$	S	2/2/2	$27.937\ [26.305, 29.569]$	S

All 48 family comparisons (continued)

	CO3Dv2			SSv2		
Condition	Choice	Margin [interval]		Choice	Margin [interval]	
T-III-Se	2/2/2	$15.561\ [10.538, 20.583]$	S	2/2/2	$21.887\ [20.112, 23.662]$	S
T-III-Cr	2/2/2	$19.387\ [14.141, 24.632]$	S	2/2/2	$35.624\ [33.700, 37.548]$	S
T-IV-Sc	1/1/1	$6.637\ [2.105, 11.170]$	S	2/2/1	$-25.442\ [-27.112, -23.773]$	F
T-IV-Se	1/1/2	$-6.949\ [-11.954, -1.944]$	F	2/2/1	$-32.787\ [-34.682, -30.893]$	F
T-IV-Cr	1/1/2	$-8.753\ [-13.955, -3.552]$	F	2/2/1	$-20.023\ [-21.974, -18.072]$	F

C.6 Complete direct comparisons

The following tables retain all 144 fit–curve–query conditions, including unchanged report choices. Absolute risks show the loss scale; the signed report contrast retains the covariance between reports. Gain compares the base-selected report with the selected report on the same query. Report and query choices are given in table 3.

Table 4: **Complete direct comparisons: CO3Dv2.** Risks are per coordinate; the paired report contrast and gain are in units of 10^{-3}. Every value gives its simultaneous 95% half-width. Query 0 is identity, F the fixed mixture and W the selected reuse witness. Report indices follow table 3.

Condition	R_0	R_1	R_2	$R_2 - R_1$	Gain
U-I-Sc-0	1.705 ± 0.031	1.088 ± 0.020	1.117 ± 0.021	29.111 ± 3.347	0
U-I-Sc-F	1.746 ± 0.032	1.116 ± 0.021	1.144 ± 0.021	28.443 ± 3.447	0
U-I-Sc-W	1.786 ± 0.033	1.148 ± 0.021	1.138 ± 0.021	-9.984 ± 3.479	9.984 ± 3.479
U-I-Se-0	1.717 ± 0.031	1.099 ± 0.020	1.129 ± 0.021	30.151 ± 3.386	0
U-I-Se-F	1.758 ± 0.032	1.130 ± 0.021	1.149 ± 0.021	18.722 ± 3.431	0
U-I-Se-W	1.795 ± 0.033	1.169 ± 0.022	1.145 ± 0.021	-23.615 ± 3.517	23.615 ± 3.517
U-I-Cr-0	1.738 ± 0.031	1.112 ± 0.020	1.138 ± 0.021	26.348 ± 3.445	0
U-I-Cr-F	1.779 ± 0.032	1.144 ± 0.021	1.156 ± 0.022	12.413 ± 3.490	0
U-I-Cr-W	1.816 ± 0.033	1.180 ± 0.022	1.156 ± 0.022	-23.832 ± 3.617	23.832 ± 3.617
U-II-Sc-0	1.714 ± 0.031	1.111 ± 0.020	1.107 ± 0.020	-3.276 ± 3.157	0
U-II-Sc-F	1.755 ± 0.032	1.138 ± 0.021	1.134 ± 0.021	-4.369 ± 3.263	0
U-II-Sc-W	1.789 ± 0.033	1.136 ± 0.021	1.173 ± 0.022	37.003 ± 3.522	37.003 ± 3.522
U-II-Se-0	1.726 ± 0.031	1.121 ± 0.020	1.119 ± 0.021	-2.824 ± 3.178	0
U-II-Se-F	1.766 ± 0.032	1.153 ± 0.021	1.138 ± 0.021	-15.007 ± 3.269	0
U-II-Se-W	1.804 ± 0.033	1.148 ± 0.021	1.191 ± 0.022	42.759 ± 3.591	42.759 ± 3.591
U-II-Cr-0	1.747 ± 0.031	1.134 ± 0.021	1.127 ± 0.021	-6.459 ± 3.252	0
U-II-Cr-F	1.787 ± 0.032	1.166 ± 0.021	1.145 ± 0.021	-21.211 ± 3.363	0
U-II-Cr-W	1.824 ± 0.033	1.157 ± 0.021	1.197 ± 0.023	39.957 ± 3.665	39.957 ± 3.665
U-III-Sc-0	1.705 ± 0.031	1.082 ± 0.020	1.114 ± 0.020	31.947 ± 3.305	0
U-III-Sc-F	1.746 ± 0.032	1.110 ± 0.020	1.141 ± 0.021	30.989 ± 3.400	0
U-III-Sc-W	1.786 ± 0.032	1.143 ± 0.021	1.136 ± 0.021	-7.300 ± 3.430	7.300 ± 3.430
U-III-Se-0	1.718 ± 0.031	1.093 ± 0.020	1.126 ± 0.021	32.904 ± 3.345	0
U-III-Se-F	1.758 ± 0.032	1.125 ± 0.020	1.146 ± 0.021	20.987 ± 3.383	0
U-III-Se-W	1.795 ± 0.032	1.164 ± 0.021	1.142 ± 0.021	-21.467 ± 3.462	21.467 ± 3.462
U-III-Cr-0	1.738 ± 0.031	1.106 ± 0.020	1.135 ± 0.021	29.060 ± 3.402	0
U-III-Cr-F	1.779 ± 0.032	1.138 ± 0.021	1.152 ± 0.021	14.558 ± 3.442	0
U-III-Cr-W	1.817 ± 0.033	1.174 ± 0.022	1.153 ± 0.021	-21.716 ± 3.570	21.716 ± 3.570
U-IV-Sc-0	1.706 ± 0.031	1.135 ± 0.021	1.106 ± 0.021	-28.274 ± 3.152	0
U-IV-Sc-F	1.747 ± 0.032	1.162 ± 0.022	1.133 ± 0.021	-29.306 ± 3.265	0
U-IV-Sc-W	1.781 ± 0.033	1.161 ± 0.022	1.174 ± 0.022	12.499 ± 3.434	12.499 ± 3.434

CO3Dv2 direct comparisons (continued)

Condition	R_0	R_1	R_2	$R_2 - R_1$	Gain
U-IV-Se-0	1.718±0.031	1.145±0.021	1.118±0.021	−27.635±3.168	0
U-IV-Se-F	1.759±0.032	1.177±0.022	1.137±0.021	−39.677±3.301	0
U-IV-Se-W	1.796±0.033	1.173±0.022	1.191±0.023	18.283±3.486	18.283±3.486
U-IV-Cr-0	1.739±0.032	1.158±0.021	1.127±0.021	−31.653±3.245	0
U-IV-Cr-F	1.779±0.033	1.190±0.022	1.144±0.022	−46.297±3.401	0
U-IV-Cr-W	1.816±0.034	1.182±0.022	1.197±0.023	15.540±3.580	15.540±3.580
T-I-Sc-0	1.706±0.031	1.120±0.020	1.110±0.020	−9.541±3.006	0
T-I-Sc-F	1.747±0.032	1.148±0.021	1.137±0.021	−11.542±3.102	0
T-I-Sc-W	1.781±0.033	1.146±0.021	1.176±0.022	30.426±3.344	30.426±3.344
T-I-Se-0	1.719±0.031	1.131±0.021	1.122±0.021	−9.539±3.022	0
T-I-Se-F	1.759±0.032	1.164±0.021	1.141±0.021	−22.520±3.114	0
T-I-Se-W	1.796±0.033	1.159±0.021	1.194±0.022	35.194±3.402	35.194±3.402
T-I-Cr-0	1.739±0.031	1.144±0.021	1.131±0.021	−13.277±3.096	0
T-I-Cr-F	1.780±0.032	1.177±0.022	1.148±0.021	−28.740±3.217	0
T-I-Cr-W	1.816±0.033	1.168±0.022	1.201±0.023	32.554±3.474	32.554±3.474
T-II-Sc-0	1.711±0.031	1.094±0.020	1.135±0.021	40.451±3.196	0
T-II-Sc-F	1.752±0.032	1.122±0.021	1.162±0.021	39.680±3.284	0
T-II-Sc-W	1.792±0.033	1.155±0.021	1.158±0.021	2.812±3.275	0
T-II-Se-0	1.723±0.031	1.105±0.020	1.146±0.021	41.090±3.246	0
T-II-Se-F	1.763±0.032	1.137±0.021	1.166±0.022	29.462±3.266	0
T-II-Se-W	1.801±0.033	1.176±0.022	1.164±0.022	−11.790±3.306	11.790±3.306
T-II-Cr-0	1.744±0.031	1.118±0.020	1.155±0.021	37.594±3.286	0
T-II-Cr-F	1.785±0.032	1.150±0.021	1.173±0.022	23.303±3.305	0
T-II-Cr-W	1.823±0.033	1.187±0.022	1.174±0.022	−12.132±3.405	12.132±3.405
T-III-Sc-0	1.712±0.031	1.169±0.021	1.116±0.020	−53.226±2.994	0
T-III-Sc-F	1.753±0.032	1.198±0.022	1.143±0.021	−55.039±3.107	0
T-III-Sc-W	1.788±0.032	1.199±0.022	1.182±0.022	−16.502±3.104	0
T-III-Se-0	1.725±0.031	1.181±0.021	1.127±0.021	−53.729±2.983	0
T-III-Se-F	1.765±0.032	1.213±0.022	1.147±0.021	−66.059±3.143	0
T-III-Se-W	1.803±0.033	1.215±0.022	1.202±0.022	−12.614±3.134	0
T-III-Cr-0	1.746±0.031	1.194±0.021	1.136±0.021	−57.854±3.082	0
T-III-Cr-F	1.786±0.032	1.227±0.022	1.154±0.021	−72.744±3.292	0
T-III-Cr-W	1.823±0.033	1.225±0.022	1.209±0.022	−16.583±3.183	0
T-IV-Sc-0	1.720±0.032	1.141±0.021	1.186±0.022	44.487±3.145	0
T-IV-Sc-F	1.762±0.033	1.169±0.022	1.214±0.023	44.652±3.242	0
T-IV-Sc-W	1.802±0.033	1.204±0.023	1.212±0.023	8.028±3.181	0
T-IV-Se-0	1.733±0.032	1.152±0.021	1.196±0.022	44.263±3.212	0
T-IV-Se-F	1.774±0.033	1.184±0.022	1.218±0.023	33.914±3.230	0
T-IV-Se-W	1.813±0.034	1.224±0.023	1.219±0.023	−5.626±3.208	5.626±3.208
T-IV-Cr-0	1.754±0.032	1.165±0.021	1.206±0.022	40.488±3.230	0
T-IV-Cr-F	1.795±0.033	1.198±0.022	1.225±0.023	27.559±3.246	0
T-IV-Cr-W	1.833±0.034	1.235±0.023	1.227±0.023	−7.648±3.310	7.648±3.310

Table 5: **Complete direct comparisons: SSv2.** Risks are per coordinate; the paired report contrast and gain are in units of 10^{-3}. Every value gives its simultaneous 95% half-width. Query 0 is identity, F the fixed mixture and W the selected reuse witness. Report indices follow table 3.

Condition	R_0	R_1	R_2	$R_2 - R_1$	Gain
U-I-Sc-0	1.687 ± 0.012	1.145 ± 0.008	1.130 ± 0.008	-14.861 ± 1.218	0
U-I-Sc-F	1.721 ± 0.012	1.172 ± 0.008	1.152 ± 0.008	-19.575 ± 1.260	0
U-I-Sc-W	1.760 ± 0.012	1.172 ± 0.008	1.196 ± 0.008	24.107 ± 1.309	24.107 ± 1.309
U-I-Se-0	1.700 ± 0.012	1.153 ± 0.008	1.141 ± 0.008	-12.772 ± 1.271	0
U-I-Se-F	1.735 ± 0.012	1.177 ± 0.008	1.169 ± 0.008	-7.542 ± 1.310	0
U-I-Se-W	1.776 ± 0.012	1.181 ± 0.008	1.210 ± 0.009	29.746 ± 1.407	29.746 ± 1.407
U-I-Cr-0	1.720 ± 0.012	1.164 ± 0.008	1.138 ± 0.008	-25.655 ± 1.281	0
U-I-Cr-F	1.755 ± 0.012	1.186 ± 0.008	1.166 ± 0.008	-20.427 ± 1.307	0
U-I-Cr-W	1.794 ± 0.012	1.189 ± 0.008	1.207 ± 0.009	17.786 ± 1.316	17.786 ± 1.316
U-II-Sc-0	1.698 ± 0.012	1.114 ± 0.008	1.144 ± 0.008	30.591 ± 1.257	0
U-II-Sc-F	1.732 ± 0.012	1.139 ± 0.008	1.166 ± 0.008	26.815 ± 1.292	0
U-II-Sc-W	1.777 ± 0.012	1.175 ± 0.008	1.167 ± 0.008	-7.944 ± 1.326	7.944 ± 1.326
U-II-Se-0	1.710 ± 0.012	1.121 ± 0.008	1.156 ± 0.008	34.479 ± 1.350	0
U-II-Se-F	1.746 ± 0.012	1.143 ± 0.008	1.184 ± 0.008	41.248 ± 1.402	0
U-II-Se-W	1.785 ± 0.012	1.186 ± 0.008	1.176 ± 0.008	-9.955 ± 1.366	9.955 ± 1.366
U-II-Cr-0	1.731 ± 0.012	1.131 ± 0.008	1.153 ± 0.008	21.430 ± 1.295	0
U-II-Cr-F	1.766 ± 0.012	1.152 ± 0.008	1.180 ± 0.008	28.414 ± 1.338	0
U-II-Cr-W	1.805 ± 0.012	1.193 ± 0.008	1.172 ± 0.008	-21.295 ± 1.421	21.295 ± 1.421
U-III-Sc-0	1.691 ± 0.012	1.143 ± 0.008	1.135 ± 0.008	-8.250 ± 1.201	0
U-III-Sc-F	1.725 ± 0.012	1.169 ± 0.008	1.157 ± 0.008	-12.436 ± 1.241	0
U-III-Sc-W	1.764 ± 0.012	1.171 ± 0.008	1.201 ± 0.008	30.153 ± 1.295	30.153 ± 1.295
U-III-Se-0	1.704 ± 0.012	1.152 ± 0.008	1.146 ± 0.008	-6.372 ± 1.252	0
U-III-Se-F	1.739 ± 0.012	1.176 ± 0.008	1.175 ± 0.008	-1.009 ± 1.292	0
U-III-Se-W	1.781 ± 0.012	1.179 ± 0.008	1.215 ± 0.009	35.469 ± 1.389	35.469 ± 1.389
U-III-Cr-0	1.724 ± 0.012	1.162 ± 0.008	1.143 ± 0.008	-18.447 ± 1.259	0
U-III-Cr-F	1.759 ± 0.012	1.184 ± 0.008	1.171 ± 0.008	-12.965 ± 1.286	0
U-III-Cr-W	1.799 ± 0.012	1.187 ± 0.008	1.211 ± 0.009	24.266 ± 1.303	24.266 ± 1.303
U-IV-Sc-0	1.689 ± 0.012	1.142 ± 0.008	1.183 ± 0.008	41.175 ± 1.151	0
U-IV-Sc-F	1.723 ± 0.012	1.169 ± 0.008	1.206 ± 0.008	37.012 ± 1.179	0
U-IV-Sc-W	1.767 ± 0.012	1.204 ± 0.008	1.210 ± 0.008	5.866 ± 1.192	0
U-IV-Se-0	1.701 ± 0.012	1.149 ± 0.008	1.195 ± 0.008	45.241 ± 1.260	0
U-IV-Se-F	1.736 ± 0.012	1.172 ± 0.008	1.224 ± 0.009	51.253 ± 1.310	0
U-IV-Se-W	1.774 ± 0.012	1.215 ± 0.009	1.220 ± 0.009	4.326 ± 1.248	0
U-IV-Cr-0	1.721 ± 0.012	1.160 ± 0.008	1.192 ± 0.008	32.102 ± 1.178	0
U-IV-Cr-F	1.757 ± 0.012	1.182 ± 0.008	1.220 ± 0.008	38.164 ± 1.220	0
U-IV-Cr-W	1.795 ± 0.012	1.223 ± 0.009	1.214 ± 0.008	-8.113 ± 1.278	8.113 ± 1.278
T-I-Sc-0	1.691 ± 0.012	1.127 ± 0.008	1.151 ± 0.008	24.693 ± 1.184	0
T-I-Sc-F	1.724 ± 0.012	1.153 ± 0.008	1.174 ± 0.008	20.816 ± 1.218	0
T-I-Sc-W	1.769 ± 0.012	1.188 ± 0.008	1.175 ± 0.008	-13.565 ± 1.260	13.565 ± 1.260
T-I-Se-0	1.703 ± 0.012	1.135 ± 0.008	1.163 ± 0.008	28.426 ± 1.265	0
T-I-Se-F	1.738 ± 0.012	1.157 ± 0.008	1.192 ± 0.009	34.792 ± 1.315	0
T-I-Se-W	1.777 ± 0.012	1.200 ± 0.008	1.184 ± 0.008	-16.121 ± 1.289	16.121 ± 1.289
T-I-Cr-0	1.723 ± 0.012	1.145 ± 0.008	1.160 ± 0.008	15.662 ± 1.223	0
T-I-Cr-F	1.758 ± 0.012	1.165 ± 0.008	1.188 ± 0.008	22.354 ± 1.264	0
T-I-Cr-W	1.797 ± 0.012	1.206 ± 0.009	1.180 ± 0.008	-26.768 ± 1.355	26.768 ± 1.355
T-II-Sc-0	1.689 ± 0.012	1.191 ± 0.008	1.187 ± 0.008	-3.818 ± 1.120	0

SSv2 direct comparisons (continued)

Condition	R_0	R_1	R_2	$R_2 - R_1$	Gain
T-II-Sc-F	1.723 ± 0.012	1.217 ± 0.008	1.210 ± 0.008	-7.624 ± 1.161	0
T-II-Sc-W	1.762 ± 0.012	1.223 ± 0.009	1.255 ± 0.009	31.696 ± 1.214	31.696 ± 1.214
T-II-Se-0	1.702 ± 0.012	1.202 ± 0.008	1.201 ± 0.008	-1.125 ± 1.168	0
T-II-Se-F	1.737 ± 0.012	1.225 ± 0.009	1.230 ± 0.009	4.871 ± 1.212	4.871 ± 1.212
T-II-Se-W	1.780 ± 0.012	1.232 ± 0.009	1.270 ± 0.009	37.973 ± 1.299	37.973 ± 1.299
T-II-Cr-0	1.722 ± 0.012	1.212 ± 0.008	1.198 ± 0.008	-13.856 ± 1.167	0
T-II-Cr-F	1.757 ± 0.012	1.233 ± 0.009	1.225 ± 0.009	-7.753 ± 1.199	0
T-II-Cr-W	1.797 ± 0.012	1.242 ± 0.009	1.267 ± 0.009	25.570 ± 1.223	25.570 ± 1.223
T-III-Sc-0	1.699 ± 0.012	1.247 ± 0.009	1.186 ± 0.008	-60.665 ± 1.170	0
T-III-Sc-F	1.733 ± 0.012	1.274 ± 0.009	1.209 ± 0.008	-65.709 ± 1.223	0
T-III-Sc-W	1.773 ± 0.012	1.282 ± 0.009	1.254 ± 0.009	-28.140 ± 1.175	0
T-III-Se-0	1.711 ± 0.012	1.257 ± 0.009	1.199 ± 0.008	-57.606 ± 1.163	0
T-III-Se-F	1.747 ± 0.012	1.280 ± 0.009	1.228 ± 0.009	-51.530 ± 1.195	0
T-III-Se-W	1.790 ± 0.012	1.291 ± 0.009	1.269 ± 0.009	-21.927 ± 1.209	0
T-III-Cr-0	1.732 ± 0.012	1.268 ± 0.009	1.196 ± 0.008	-71.948 ± 1.249	0
T-III-Cr-F	1.768 ± 0.012	1.289 ± 0.009	1.223 ± 0.009	-65.534 ± 1.259	0
T-III-Cr-W	1.808 ± 0.012	1.301 ± 0.009	1.265 ± 0.009	-35.815 ± 1.205	0
T-IV-Sc-0	1.688 ± 0.012	1.159 ± 0.008	1.145 ± 0.008	-13.587 ± 1.160	0
T-IV-Sc-F	1.722 ± 0.012	1.186 ± 0.008	1.167 ± 0.008	-18.186 ± 1.200	0
T-IV-Sc-W	1.762 ± 0.012	1.186 ± 0.008	1.211 ± 0.009	25.032 ± 1.250	25.032 ± 1.250
T-IV-Se-0	1.701 ± 0.012	1.167 ± 0.008	1.157 ± 0.008	-9.780 ± 1.209	0
T-IV-Se-F	1.736 ± 0.012	1.190 ± 0.008	1.186 ± 0.008	-3.944 ± 1.249	0
T-IV-Se-W	1.778 ± 0.012	1.193 ± 0.008	1.226 ± 0.009	32.539 ± 1.345	32.539 ± 1.345
T-IV-Cr-0	1.721 ± 0.012	1.177 ± 0.008	1.154 ± 0.008	-23.464 ± 1.217	0
T-IV-Cr-F	1.756 ± 0.012	1.199 ± 0.008	1.181 ± 0.008	-17.160 ± 1.243	0
T-IV-Cr-W	1.797 ± 0.012	1.202 ± 0.008	1.222 ± 0.009	19.612 ± 1.258	19.612 ± 1.258